Targeting OCA-B/Pou2af1 blocks type-1 diabetes and reduces infiltration of activated, islet-reactive T cells

Heejoo Kim[1,2], Jelena Perovanovic[1,2], Arvind Shakya[1,2], Zuolian Shen[1,2], Cody German[1,2], Andrea Ibarra[1,2], Jillian L. Jafek[1,2], Nai-Pin Lin[3], Brian D. Evavold[1], Danny H.-C. Chou[3], Peter E. Jensen[1], Xiao He[1], and Dean Tantin[1,2,*]

[1]Department of Pathology, University of Utah School of Medicine, Salt Lake City, UT 84112, U.S.A.
[2]Huntsman Cancer Institute, University of Utah School of Medicine, Salt Lake City, UT 84112, U.S.A.
[3]Department of Biochemistry, University of Utah School of Medicine, Salt Lake City, UT 84112, U.S.A.

[*]Corresponding authors: Dean Tantin, Department of Pathology, University of Utah School of Medicine, Salt Lake City, UT 84112. E-mail address: dean.tantin@path.utah.edu

Other authors: Heejoo Kim, heejoo.kim@path.utah.edu;

Running title: OCA-B in T1D

Manuscript data:
Characters in title (including spaces): 108
Words in abstract: 261
Character count (including spaces):
Total main figures: 7
Total main tables: 0

Abstract

Autoimmune therapies aim to inhibit autoreactivity while preserving normal immune function. The transcriptional coregulator OCA-B, also known as Bob.1/OBF-1 (gene symbol *Pou2af1*) is induced in stimulated naïve CD4$^+$ T cells, where docks with transcription factor Oct1 to regulate genes such as *Il2* and *Ifng*. OCA-B regulates its targets in cases of repeated antigen exposure, a necessary feature of autoimmunity. Polymorphisms in binding sites for Oct1, and by extension OCA-B, as associated with multiple forms of autoimmunity including autoimmune (type-1) diabetes. We hypothesized that T cell-specific OCA-B deletion would protect mice from type-1 diabetes, and that pharmacologic OCA-B inhibition would provide similar protection. We developed an *Ocab* (*Pou2af1*) conditional allele and backcrossed it onto a diabetes-prone NOD/ShiLtJ strain background. T cell-specific OCA-B loss protected mice from spontaneous T1D. Protection was associated with reduced pancreatic T cell and macrophage infiltration and reduced proinflammatory cytokine expression. We profiled prediabetic pancreatic lymph nodes and islets by single-cell RNA sequencing and T cell receptor clonotype analysis. Although lymph nodes showed minimal differences, activated/memory CD8$^+$ cell specificities known to participate in diabetes pathogenesis failed to emerge in the islets of OCA-B deficient mice. In contrast, CD4$^+$ clones associated with diabetes were present, but only in anergic cells. The protective effect of OCA-B loss was diminished, or even eliminated, using monoclonal models with high affinity to artificial or neoantigens. Rationally-designed membrane-penetrating OCA-B peptide inhibitors normalized glucose levels, and reduced T cell infiltration and proinflammatory cytokine expression in newly-diabetic NOD mice. Together, the results indicate that OCA-B is a potent autoimmune regulator and a promising target for pharmacologic inhibition.

52 **Introduction**

53 Type 1 Diabetes (T1D) is an autoimmune disease in which the host immune system is directed towards
54 antigens associated with pancreatic beta cells [1, 2]. Pathologically, T1D is characterized by insulitis, beta
55 cell destruction and consequent inability to produce insulin. The main treatment for T1D, life-long
56 insulin therapy, treats symptoms but not cause. The development of new T1D treatments is limited by
57 an incomplete understanding of disease mechanisms [3]. Beta cell regeneration is a promising line of
58 therapy, but is likely to result in renewed autoimmune attack unless methods can be developed to
59 specifically block T1D autoimmunity. An ideal method of therapy would be to capture patients early in
60 the disease course and block autoimmunity while keeping normal immune function intact. Such a
61 therapy would spare remaining beta cell function.

62 In $CD4^+$ T cells, the transcription factor Oct1 and its cofactor OCA-B regulate a set of ~150
63 target genes, including *Il2*, *Ifng* and *Csf2* (*Gmcsf*) [4]. Upon T cell activation, many of these targets are
64 activated by pathways that converge on transcription factors such as NF-AT, AP-1 and NF-κB. Factors
65 like NF-AT can be thought of as the primary on/off switches for these genes, and drugs that block NF-
66 AT activation effectively shut down target gene expression. Such drugs have utility in many contexts,
67 but also have drawbacks including global dampening of immune function and side effects due to
68 expression in other tissues. In contrast, Oct1 and OCA-B insulate silent but previously activated target
69 genes against stable repression. Loss of either protein does not affect $CD4^+$ T cell responses to
70 stimulation in vitro or primary infection in mice [4, 5], but causes large defects in target gene expression
71 (100-fold or more) upon secondary stimulation and causes defective $CD4^+$ memory T cell formation
72 and recall responses [4, 6]. In addition, OCA-B expression is largely confined to lymphocytes. OCA-B is
73 silent in thymocytes and naïve $CD4^+$ T cells, but is induced and stably expressed after sustained
74 antigen stimulation [4]. Once expressed, OCA-B recruits the histone lysine demethylase
75 Jmjd1a/Jhdm2a/Kdm3a to Oct1 at target loci, where it locally removes inhibitory H3K9me2 chromatin
76 marks that would otherwise promote repressive chromatin environments [4, 6]. OCA-B also potentiates
77 polarization of activated helper T cells towards the Th17 phenotype, among the most pro-inflammatory
78 helper T cell subsets [7].

79 Persistent antigen exposure is also a common property of autoimmune responses. Among
80 profiled $CD4^+$ T cell subsets, OCA-B levels are elevated in both central memory cells and pancreas-
81 infiltrating, islet-reactive cells (http://www.immgen.org/databrowser/index.html). Both Oct1 and OCA-
82 B are highly conserved to humans, and genome-wide association studies identify Oct1/OCA-B binding
83 site polymorphisms that confer predisposition to a variety of human autoimmune diseases including

84 type-1 diabetes (T1D), multiple sclerosis, lupus, inflammatory bowel disease and rheumatoid arthritis
85 [8, 9, 10, 11, 12, 13, 14]. Other studies implicate polymorphisms in or near the *Ocab* (*Pou2af1*) locus itself in
86 different forms autoimmunity [15, 16]. We therefore hypothesized that targeting OCA-B would inhibit
87 over-active, diabetogenic T cell responses.

88 Here, we generated a T cell conditional mouse model of OCA-B deficiency. We show that
89 OCA-B ablation protects animals from spontaneous, polyclonal T1D. Protection was associated with
90 reduced T cell infiltration and proinflammatory cytokine expression. Conditional OCA-B deletion
91 maintained normal pancreatic lymph node cell populations, numbers, gene expression and TCR
92 clonality, however deletion in the prediabetic pancreas was associated with significant alterations in
93 specific TCR clones. Protection from OCA-B loss varied among different TCR transgenic and
94 monoclonal antigen models, and was weakest using synthetic antigens and monoclonal transplant
95 models. Protection was stronger, but still incomplete, using a spontaneous CD8 TCR transgenic model.
96 Using a rational-design approach, we developed membrane-penetrating OCA-B peptide inhibitors that
97 are efficacious in vitro and in mice. Cumulatively, the results indicate that OCA-B is a potent and
98 pharmacologically accessible autoimmune regulator.

99 **Results**

100 **Generation of an *Ocab* conditional allele and NOD backcrossing.** We generated a conditional *Ocab*
101 (*Pou2af1*) mouse allele using embryonic stem cells provided by the knockout mouse project (KOMP)
102 repository. Deletion of the *LoxP* sites is predicted to create a null allele by disrupting the first three
103 exons (Fig. 1a). Breeding chimeric mice resulted in germline transmission and a founder mouse (Fig.
104 1B, lane 2) that was crossed to a FLP deleter mouse strain (*Rosa26*-FLP) to remove the reporter
105 cassette and create a floxed conditional allele (Fig. 1a and b, lane 3). Intercrossing these mice
106 generated homozygous *fl/fl* mice (Fig. 1b, lane 4). The mice were crossed to germline Cre deleter mice
107 (Rosa26-Cre) to generate null (*Δ*) alleles (lanes 5 and 6). As expected, homozygous *fl/fl* mice produce
108 normal amounts of both p34 and p35 OCA-B protein isoforms (Supplementary Fig. 1a, lane 6), while
109 no protein of either isoform is present in germline-deleted *Δ/Δ* spleens (lanes 7-8). These results
110 indicate that the *fl* allele is OCA-B sufficient and the Cre-deleted allele is a null. Crossing the *fl* allele
111 onto a Cre^{CD4} driver, which deletes in both CD4 and CD8 compartments, resulted in efficient deletion
112 in splenic T cells (Fig. 1b). These findings indicate that this allele represents a robust system in which
113 to study OCA-B function in T cells.

114 The *Ocab* (*Pou2af1*) conditional allele was generated on a C57BL/6 background. To test the
115 prediction that OCA-B expression in T cells promotes T1D emergence, we conducted speed congenic
116 backcrosses to the NOD strain background. This method allows spontaneous diabetes to be produced
117 rapidly by screening and selecting for 13 microsatellite and SNP markers associated with NOD
118 autoimmune susceptibility [17]. Backcrossing is facilitated by the fact that *Ocab* is located on mouse
119 chromosome 9 and is not nearby any of the *Idd* loci. Following these markers with specific primer
120 pairs (Supplementary Table 1), we produced backcrossed animals with all 13 markers (Supplementary
121 Fig. 1b) that recapitulate spontaneous autoimmunity (not shown). For example, *Idd1*, which maps to
122 the MHC region [18], converted to the homozygous NOD allele after 2 backcross generations
123 (Supplementary Fig. 1B, lane 3), whereas *Idd13*, which maps near beta-2-microglobulin [19] became
124 NOD homozygous after 4 generations (lane 4). Genotyping identified this fourth-generation
125 backcrossed animal as having all 13 microsatellite markers and the *Ocab* conditional allele
126 (Supplementary Fig. 1c, #122). This founder animal was crossed to NOD.Cre^{CD4} and the floxed allele
127 homozygosed in order to delete OCA-B in T cells to assess the effects on T1D. Similar NOD
128 backcrosses, conducted using *Ocab* null mice [20], resulted in OCA-B germline-deficient NOD mice
129 (data not shown). As with the original C57BL/6 OCA-B germline knockout [20], all alleles were viable
130 and fertile with no obvious health issues.

131

132 **NOD mice lacking OCA-B are protected from T1D.** To study the effect of T cell-specific OCA-B
133 loss on baseline immune function, we performed single-cell RNA sequencing (scRNAseq) and TCR
134 clonotype analysis using $CD3^+$ T cells isolated from PLNs of pre-diabetic 8 week-old female
135 NOD.*Ocab*$^{fl/fl}$Cre^{CD4} or NOD.*Ocab*$^{fl/fl}$ littermate controls. For each group cells from three animals were
136 combined for microfluidics and subsequent sequencing. T cells were isolated from PLNs of three
137 animals in each group and combined for analysis. ~6000 knockout and ~3000 control cells were
138 identified in this analysis, most of which comprise naïve CD4 and CD8 cells (Supplementary Fig. 2a,
139 pink and orange), and regulatory T cells (Tregs, green). There was also a small population of activated
140 $CD4^+$+$CD8^+$ cells (green), presumably in the process of exiting the lymph nodes. Other than a small
141 decrease in the percentage of activated $CD4^+$+$CD8^+$ cells (4.4 vs 6.1%), few differences in the
142 populations were observed. None of these populations expressed measurable amounts of *Ocab*
143 (*Pou2af1*) mRNA (not shown), however *Pou2af1* is expressed at low levels in T cells making it
144 difficult capture by scRNAseq. In addition, few changes in gene expression were identified, and the
145 great majority of these were not of immunological interest (Supplementary Fig. 2b, Supplementary
146 Table 2). We also determined TCR repertoires in these T cell populations, identifying few changes as a
147 whole (Supplementary Fig. 2c) or in specific sub-populations (not shown). These results indicate that
148 OCA-B loss does not have obvious effects on PLN T cell repertoires or status.

149 T1D onset in NOD mice is spontaneous and acute [21]. To test the impact of OCA-B loss in T
150 cells on spontaneous T1D, we compared incidence in in female NOD.*Ocab*$^{fl/fl}$Cre^{CD4} mice, and controls
151 lacking the Cre^{CD4} driver. Glucose was monitored 2-3 times per week. Using a 250 mg/dL blood
152 glucose cutoff, approximately 60% of *Ocab*$^{fl/fl}$ control mice manifested spontaneous diabetes by 24
153 weeks of age, while no *Ocab*$^{fl/fl}$Cre^{CD4} mice became diabetic (Fig. 1d). Blood glucose was stable in
154 *Ocab*$^{fl/fl}$Cre^{CD4} females but began to spike in control mice beginning at week 16, rising to an average of
155 >300 mg/dL by 24 weeks (Fig. 1e). Similar results were observed using female whole-body knockout
156 NOD.*Ocab*$^{-/-}$ compared to *Ocab*$^{+/+}$ littermate controls. While ~80% of control females developed T1D
157 within 24 weeks after birth, only ~20% of NOD.*Ocab*$^{\Delta/\Delta}$ females did so (Fig. 1f). Cumulatively, the
158 results show that OCA-B expression in T cells is critical for T1D pathogenesis in NOD mice.

159

160 **NOD.*Ocab* conditional mice have fewer islet macrophages and IFNγ–expressing cytotoxic T cells,**
161 **and more Tregs.** We sacrificed *Ocab*$^{fl/fl}$Cre^{CD4} female mice and controls at 8 and 24 weeks, and
162 determined the frequencies of immune cells in the pacreata. We observed more T cells in the pancreata

163 of OCA-B deficient mice (not shown). This result is understandable because the control mice have
164 annihilated their pool of beta cells, resulting in lack of antigen. We also studied pancreatic
165 macrophages in these mice. Islet infiltration of F4/80^{+}CD11b^{+} macrophages is critical for NOD T1D
166 pathogenesis both in spontaneous and adoptive transfer T1D models [22, 23]. CCL1 expressed in
167 diabetogenic CD4 T cells is known to recruit CCR8-expressing macrophages [24]. Interestingly, OCA-B
168 deletion in stimulated, rested and re-stimulated CD4^{+} T cells decreases *Ccl1* mRNA expression
169 compared to controls (Supplementary Table 3). We therefore hypothesized that OCA-B expression in
170 T cells is important for macrophage islet infiltration. Despite the fact that antigen and greater numbers
171 of T cells were present, we observed 5-fold fewer macrophages in 24 week-old NOD.*Ocab*$^{fl/fl}$Cre^{CD4}
172 islets (Fig. 2a,b). In contrast, macrophage numbers were unaffected by T cell-specific OCA-B loss in
173 pre-diabetic (8 week) mice (Fig. 2a).

174 IFNγ is a direct OCA-B target gene [4] and a strong promoter of T1D. Levels of serum and
175 pancreatic IFNγ gradually rise in young NOD mice, reaching maximum at diabetes onset [25].
176 Diabetogenic CD4^{+} and CD8^{+} T cells both express IFNγ in humans and NOD mice [26, 27, 28]. Therefore,
177 we predicted that OCA-B loss would reduce islet IFNγ expression in CD4^{+} and CD8^{+} T cells. We
178 compared IFNγ-expressing pancreatic CD4^{+} and CD8^{+} T cells in female NOD.*Ocab*$^{fl/fl}$Cre^{CD4} and
179 littermate control mice lacking Cre^{CD4}. In 12 week-old prediabetic mice, CD8^{+} T cell frequencies were
180 significantly decreased (Fig. 2c), whereas CD4^{+} T cells at the same timepoint were unchanged (data
181 not shown). At the time of diabetes onset (16 weeks), proportionally fewer IFNγ-expressing CD8^{+} T
182 cells were present in *Ocab* conditional-deleted mice compared to controls (Fig. 2d).

183 CD4^{+}CD25^{HI}FoxP3^{+} Tregs interfere with T1D development in NOD mice [29, 30]. Analysis of
184 previously generated RNAseq datasets shows that naïve *Ocab* null CD4^{+} T cells express 4-fold more
185 *Foxp3* mRNA compared to controls upon in vitro stimulation (Supplementary Table 3). To determine
186 whether the protection conferred by T cell conditional OCA-B is associated with changes in Tregs, we
187 analyzed pancreatic Treg frequencies, observing a trend towards more Tregs in pre-diabetic (8 week-
188 old) NOD.*Ocab*$^{fl/fl}$Cre^{CD4} mice compared to controls (Fig. 2e). Interestingly, there were no differences
189 late in disease course, at 16 or 24 weeks (data not shown).

190 If increased Treg numbers help mediate protection in NOD.*Ocab*$^{fl/fl}$Cre^{CD4} mice, then depletion
191 of these Tregs would be expected normalize T1D pathogenesis in knockout mice relative to controls.
192 Anti-CD25 antibody injection in neonatal mice preferentially depletes Tregs and accelerates T1D onset
193 in NOD mice [31]. Surprisingly, we observed that anti-CD25 antibody-injected NOD.*Ocab*$^{fl/fl}$Cre^{CD4} mice
194 were still protected from T1D development relative to controls, though to a lesser degree than in

195 undepleted mice (Fig. 2f). These results support a conclusion that Tregs partly contribute to the T1D
196 protection in mice lacking OCA-B in their T cells.
197
198 **T cell-specific OCA-B deletion alters the islet-infiltrating TCR repertoire.** We performed
199 scRNAseq and TCR clonotype analysis similar to Supplementary Fig. 2, but using older (12 week) but
200 still pre-diabetic NOD.*Ocab*$^{fl/fl}$Cre^{CD4} or NOD.*Ocab*$^{fl/fl}$ littermate control female mice, and using total
201 CD45^{+} cells isolated from pancreatic islets rather than PLNs. Cells were isolated from four animals per
202 group and combined for microfluidics and sequencing. After filtering, ~6200 knockout and ~3800
203 control cells were identified. Overlaying cell from both genotypes, we used their gene expression
204 profiles to definitively identify multiple cell lineages, including naïve CD4^{+} + CD8^{+} T cells,
205 memory/effector CD4^{+} T cells, memory/effector CD8^{+} T cells, B cells, macrophages and neutrophils
206 (Fig. 3a). The biggest relative change in populations was neutrophils, which decreased from 3.4 to
207 1.4% in conditional knockout iselts (Fig. 3a). B cells were also decreased, albeit more slightly. These
208 changes were accompanied by an increase in the percentages of CD4^{+} and CD8^{+} T cells with naïve
209 phenotypes in conditional knockouts (31.7 vs. 25%). Like endpoint diabetic animals (Fig. 2a,b),
210 macrophage numbers were decreased but only slightly. Unlike PLNs, prediabetic islets showed
211 significant changes in gene expression between the two groups (Fig. 3b), the strongest of which
212 occurred in neutrophils (e.g., *Cxcl2*, down), memory/effector CD8^{+} T cells (*Ccl4*, *Tcrg-v1*, *Itga*, down;
213 *Tcrbv1*, *Trav8n-2*, up), NK T cells (*Klra2*, *Lars2*, down) and γδT cells (*Gzma*, *Gzmb*, *Ccl5*, down).
214 We also profiled TCR clonality in pancreatic T cells. Across total T cells, few changes were
215 observed (Supplementary Fig. 3), however this was largely to do similar representation in the naïve T
216 cell pool. Isolating just antigen-experienced CD4^{+} and CD8^{+} effector + memory subpopulations
217 revealed sharp differences. For example, polyclonal NOD mice CD8^{+} T cells expressing *Trbv13-3*
218 (Vβ8.1) display reactivity to insulin gene related peptide (IGRP) and are associated with T1D [32].
219 Relative to controls, this clone was under-represented in OCA-B deficient effector + memory CD8^{+}
220 cells (Fig. 3c, 20.9% vs 8.6%). Based on this information, we repeated the clonotype analysis, but only
221 using the effector + memory CD8^{+} T cell cluster. Within this population, dominant TCR clonotypes
222 used by conditional and control T cells were strikingly different (Fig. 3d). Clonotype 1 for example
223 corresponds to a TCRα V8N-2 chain paired with TCRβ V1 or V15 and is not associated with T1D.
224 This clonotype was absent in control islets but represented >4% of OCA-B deficient islet CD8^{+}
225 effector + memory T cells (Fig. 3d). Clonotype 1 cells overlaid with both genotypes is shown in Fig.
226 3e. Clonotype 2 by contrast is associated with the T1D-associated Vβ13.3 β chain. This clonotype was

227 strongly represented in controls (>3%) but absent from experimental effector + memory $CD8^+$ cells
228 (Fig. 3d). In contrast to CD8-dominant TCR clonotypes, CD4-dominant TCRs associated with T1D
229 were still present in knockouts, but associated with markers of anergy. For example, clonotype 4
230 (*Trav13-1/16N+Trbv15*) is associated with pro-diabetogenic, BDC-reactive $CD4^+$ T cells [33]. This
231 clonotype was enriched in the OCA-B deficient effector + memory $CD4^+$ cells, but only in a CTLA4-
232 and FR4-expressing sub-population (Fig. 3e). Cumulatively, these results indicate that OCA-B loss
233 from T cells signicantly skews the landscape of islet effector/memory-like T cells, in particular $CD8^+$ T
234 cells, to an anti-diabetogenic phenotype.
235
236 **Protection conferred by OCA-B loss is model-specific.** T1D in NOD mice originates from defective
237 negative selection in developing T cells, resulting in T cell autoreactivity. OCA-B is not expressed in
238 thymocytes and OCA-B loss does not appear to affect T cell development [4]. Therefore, the protective
239 effect of OCA-B loss in T cells likely arises from blunting pre-existing autoreactivity in the periphery.
240 To test the hypothesis that OCA-B loss confers protection in simplified systems, we crossed OCA-B
241 deficient mouse models employing TCR transgenes and model antigens.
242 Depleting Tregs and transferring remaining T cells from BDC2.5 TCR transgenic mice into
243 NOD.Scid mice results in disease after approximately 10 d [34, 35]. We crossed the germline null *Ocab*
244 allele to BDC2.5 mice to test the effect of OCA-B in this model. We transferred $CD4^+CD25^-$ T cells
245 from germline $Ocab^{-/-}$ or $Ocab^{+/+}$ BDC2.5 mice into NOD.Scid recipients, monitoring diabetes
246 emergence. Transplants from both $Ocab^{-/-}$ and control NOD.BDC2.5 mice resulted in equivalent
247 disease kinetics (Fig. 4a) and severity (not shown). Transferring $CD4^+CD62L^+V\beta^+$ T cells from $Ocab^{-/-}$
248 and control NOD.BDC2.5 mice into NOD.Scid recipients also showed no difference between the
249 experimental and control groups (Supplementary Fig. 4a). Negative results were also generated by
250 transplanting total $CD4^+$ T cells into immunodeficient NCG recipients (Fig. 4b). We also tested the
251 effect of T cell conditional OCA-B deletion in a different strain background, C57BL/6J, using the
252 artificial membranous ovalbumin antigen expressed from the rat insulin promoter (RIP-mOVA) [36]. In
253 this experiment, wild-type OVA-reactive $CD8^+$ OT-I T cells were transferred into either $Ocab^{fl/fl}Cre^{CD4}$
254 or control $Ocab^{fl/fl}$ RIP-mOVA mice. Host $CD4^+$ T cells help transferred OT-I T cells promote T1D
255 pathogenesis in this model [37]. Mice were then infected with Lm-OVA to induce strong and
256 synchronous beta cell destruction and loss of glucose control (>400 mg/dL). No differences were
257 observed (Supplementary Fig. 4b). These results indicate that OCA-B does not act analogously to
258 transcription factors that act as a primary on/off switches, such as NF-AT. Knockouts of these factors

259 would result in broad immunosuppression and protection from T1D in all models. Rather, our results
260 suggest that the effects of OCA-B loss may protect from autoimmunity in specifc contexts, including
261 polyclonal contexts. To test this supposition, we also performed transplant experiments using total
262 splenocytes from polyclonal NOD.*Ocab*$^{fl/fl}$Cre^{CD4} mice or controls. Using this transplant system, robust
263 T1D protection with T cell-specific OCA-B loss was observed (Fig .3c). This protection was
264 associated with fewer IFNγ-expressing cytotoxic T cells were detected in the islets of OCA-B T cell
265 conditional NOD mice (Fig. 4d).
266 NY8.3 transgenic mice express a CD8-restricted TCR directed towards IGRP$_{206-214}$ and
267 manifest spontaneous T1D [38]. The NY8.3 clonotype was significantly attenuated in the islets of T cell
268 conditional OCA-B deficient mice (Fig. 3c,d,e). We also crossed the *Ocab* germline allele NY8.3,
269 passively monitoring *Ocab*$^{-/-}$ or littermate control *Ocab*$^{+/+}$ NY8.3 mice for T1D development.
270 Significant protection was observed (HR=0.4472, p=0.0352), though the degree of protection was less
271 than in polyclonal models (Fig. 4e). Together with the observed depletion of autoreactive CD8 clones
272 from OCA-B deficient pancreatic islets, this result indicates that OCA-B promotes T1D in peripheral
273 auto-reactive T cells in part directly through through the CD8$^+$ cells. Using immunoblotting with OCA-
274 B antibodies, we confirmed OCA-B expression in primary splenic C57BL/6 CD8$^+$ T cells. OCA-B is
275 undetectable in naïve splenic CD4$^+$ cells but becomes induced with prolonged activation [4]. Unlike
276 CD4$^+$ cells (Fig .4f, top panels), OCA-B$^+$ could be detected in naïve cells (Fig. 4f, lane 1). Expression
277 was augmented more rapidly in CD8$^+$ cells upon T cell activation using CD3ε/CD28 antibodies (lane
278 2). Similar to CD4$^+$ cells, expression was stably maintained when the stimulus was removed and cells
279 were rested with IL-2 (lane 6).
280
281 **OCA-B deficiency promotes CD4$^+$ T cell anergy in vitro.** Our scRNAseq data indicate that CD8-
282 restricted clones associated with T1D are depleted from the islets of OCA-B T cell conditional mice. In
283 contrast, CD4-restricted clones were increased but associated with an anergic phenotype (Fig. 3e).
284 Anergy is a peripheral tolerance mechanisms in which T cells that encounter TCR signals without co-
285 stimulation become nonfunctional to protect from autoreactivity [39, 40, 41]. Normal naïve primary CD4$^+$ T
286 cells can be activated in culture by TCR and costimulatory receptor activation, e.g. with anti-
287 CD3ε/CD28 antibodies. Providing TCR signals (via immobilized anti-CD3ε monoclonal antibodies) to
288 naïve T cells in culture generates anergic responses [42]. Loss of Oct1, the transcription factor with
289 which OCA-B docks, augments anergic responses in this assay [5]. To determine if OCA-B loss
290 similarly promotes anergic CD4$^+$ T cell responses, we stimulated naïve splenic CD4$^+$ T cells from

291 germline knockout *Ocab*$^{-/-}$ and control *Ocab1*$^{+/+}$ animals for 48 hr ex vivo using plate-bound anti-
292 CD3ε antibodies without co-stimulation, and restimulated the cells with PMA/ionomycin. Following
293 restimulation, CD4^{+} T cells lacking OCA-B generated 2.5-fold less IL-2 (Fig. 5a,b), indicating that
294 OCA-B provides a barrier against anergic responses.

295 ICOS (Inducible T-cell Costimulator) has an important role in the induction of T cell anergy
296 and is down-regulated by Oct1 loss in T cells [43, 44, 45]. Similarly in CD4^{+} cells, elevated expression of
297 FR4 and CD73 is associated with anergy and higher in Oct1-deficient compared to control cells [39, 46].
298 To determine whether OCA-B affects in the protein related to T cell anergy, we harvested pre-
299 activated CD4^{+}CD44^{+} T cells from the spleens of *Ocab*$^{fl/fl}$Cre^{CD4} and littermate control Cre^{CD4} animals,
300 and re-stimulated them for 24 hr ex vivo using anti-CD3ε antibodies ± co-stimulation using anti-CD28
301 antibodies. CD4^{+}CD44^{+}FR4^{hi}CD73^{hi} anergic cells were ~2 fold more strongly induced in T cells
302 lacking OCA-B (Fig. 5c). ICOS levels were similarly elevated in the OCA-B deficient condition (Fig.
303 5d). Additionally, and consistent with prior data [5], the expression of the activation marker CD25 was
304 decreased (Fig. 5e). These results suggest that OCA-B loss creates a requirement for CD28 co-
305 stimulation in secondary stimulation situations, effectively instituting higher immune checkpoint
306 thresholds in order for cells to become fully re-activated.
307

308 **Generation of an OCA-B peptide inhibitor.** The normal T cell developmental and primary immune
309 response phenotypes observed with OCA-B genetic deletion suggested the possibility of a "therapeutic
310 window" in which targeting OCA-B pharmacologically would leave baseline immune function only
311 minimally affected. Drugs that target transcription factors and protein-protein interactions are now
312 entering clinical use [47, 48]. Pre-clinical membrane-penetrating peptides have also been developed that
313 successfully target transcription factors such as BCL6 [49]. Based on the co-crystal structure of the Oct1
314 DNA-binding domain, the OCA-B N-terminus and consensus binding DNA [50], we applied rational-
315 design principles to generate a membrane-permeable peptide inhibitor of OCA-B's downstream
316 effector functions in order to target OCA-B pharmacologically.

317 In CD4^{+} T cells, Oct1 interacts with Jmjd1a in a MEK/ERK-dependent manner [4, 6]. Oct1
318 contains two consensus ERK phospho-acceptor serines. The structure of the Oct1 DNA binding
319 domain complexed with consensus octamer binding site DNA [51] reveals that these Oct1 serines are
320 located in a flexible, solvent-exposed loop (the linker domain), which connects the two DNA binding
321 sub-domains (Fig. 6a, red dashed line). In contrast with Oct1, OCA-B constitutively interacts with
322 Jmjd1a [4]. The OCA-B N-terminus has been solved in complex with Oct1 and consensus octamer DNA

323 [50]. The crystalized region of OCA-B is known to include regions critical for both Oct1 binding and
324 transcription activity [52]. To identify potential Jmjd1a-interacting OCA-B regions, we aligned the full-
325 length Oct1 and OCA-B amino acid sequences to a region of androgen receptor (AR) known to interact
326 with Jmjd1a [53]. Human AR mutations that cause androgen insensitivity have been mapped to a cofactor
327 interaction surface spanning residues 698-721 [54]. Aligning this sequence to full-length Oct1 identified
328 the linker domain as the top hit (Fig. 6b), implicating the Oct1 linker as a potential Jmjd1a-interacting
329 surface. The alignment shows conservation of 3 out of 4 sites of deleterious AR mutation (asterisks)
330 with Oct1. The mutation site that is not conserved is a consensus ERK target in Oct1, and a phospho-
331 mimetic glutamic acid residuein AR (blue box). These findings suggest that the Oct1 linker domain
332 constitutes a surface which, when phosphorylated by ERK, interacts with Jmjd1a.
333 As with Oct1, alignment with OCA-B identifies a potential Jmjd1a interacting surface (Fig.
334 6b). Unlike Oct1, an OCA-B glutamic acid residue (Glu30) aligns with AR, consistent with the finding
335 that OCA-B constitutively interacts with Jmjd1a in the absence of ERK signaling [4]. Furthermore, the
336 OCA-B residues aligning to AR lie on one side of a short, solvent-exposed alpha-helix (Fig. 6a). Glu30
337 (red), Leu31 (yellow), Arg34 (blue) and His38 (blue) may therefore constitute a Jmjd1a docking
338 surface. These residues are conserved to humans (Fig. 6c). We mutated OCA-B L31 and R34 to
339 alanines in a transient expression plasmid to test the effect on the Jmjd1a interaction, and transfected
340 the double-point mutant or parent plasmid control into HCT116 cells, which do not express
341 endogenous OCA-B. Control co-IP using Jmjd1a antibodies and wild-type OCA-B confirms the
342 published interaction (Fig. 6d, lane 5), while the mutant OCA-B protein failed to interact (lane 8). The
343 mutant was expressed equivalently to WT in HCT116 cells (lanes 2, 3). These results show the
344 importance of OCA-B residues 30-38 for the interaction with Jmjd1a.
345 To identify potential OCA-B competitive inhibitors, we synthesized three overlapping peptides
346 corresponding to the OCA-B N-terminus (Fig. 6e, peptides #1, #2 (hereafter called "JumOCA") and
347 #3), as C-terminal fusions to the HIV Tat protein for membrane permeability [55]. Initial preparations
348 were conjugated to FITC to track the peptide. Incubating peptides with total splenic or pancreatic
349 $CD3^+$ T cells in culture with 45 μM Tat-fused peptide for 15 min resulted in significant concentration.
350 Control OVA-fused peptide showed no such effect (Supplementary Fig. 5). We then treated splenic
351 $CD4^+$ T cells with the Tat-fused peptides (lacking FITC) in ex vivo culture. Prior work has shown that
352 6 hr restimulation of resting but previously activated cells reveals sensitivity to OCA-B loss [4]. Using
353 this assay with 50 μM JumOCA peptide (every other day with media changes during rest and
354 restimulation) inhibited *Il2* mRNA expression relative to β-actin by ~10-fold (Fig. 6f, compare Tat

355 peptide to JumOCA). Although treated cells showed no obvious changes in viability, morphology or
356 expansion during the course of the assay (not shown), there was a 2-3-fold nonspecific diminution of
357 activity associated with unfused Tat peptide (Fig. 6f, compare Tat peptide with no peptide). The Tat
358 membrane-penetrating peptide has been associated with toxicities [49, 56, 57]. Similar results were obtained
359 with the larger peptide #3 but not with peptide #1 (not shown). Peptide #1 is missing residues
360 important for the Jmjd1a interaction based on mutagenesis (Fig. 6b). For all further experiments, we
361 exclusively used the JumOCA peptide.
362 We then synthesized a Tat-conjugated peptide using a scrambled JumOCA sequence. This
363 peptide has the same amino acid composition, mass and pI, but lacks the OCA-B primary amino acid
364 sequence and should not be able to efficiently complete for Jmjd1a. We used the Tat-only, scrambled
365 and JumOCA peptides in assays similar to Fig. 6f, except using flow cytometry to assay endpoint IL-2
366 production. JumOCA significantly inhibited IL-2 production relative to the scrambled control,
367 however there were significant toxicities associated with both the scrambled and Tat-only peptides
368 relative to vehicle (Fig. 6g). A example mouse from this experiment is shown in Fig. 6h.
369 The above results are consistent with the JumOCA peptide operating through a Jmjd1a
370 competitive inhibition mechanism. To test this directly, we used JumOCA (lacking Tat) in a Jmjd1a
371 co-IP assay. We subjected lysates from mouse M12 B cells, which expresses endogenous OCA-B, to
372 immunoprecipitation with Jmjd1a antibodies, resulting in efficient OCA-B co-IP (Fig. 6g, lane 3).
373 Compared to vehicle control, (lane 3), application incubation of immunoprecipitate with JumOCA at
374 concentrations as low as 1.25 μg/mL completely eliminated the Jmjd1a-OCA-B interaction (lane 4).
375
376 **An OCA-B peptide inhibitor protects NOD mice from newly-arisen diabetes.** By the time
377 symptoms arise in NOD mice, 90-95% of beta cells have been destroyed. Remaining beta cells are
378 rendered nonfunctional due to insulitis. Alleviating this inflammation provides a "honeymoon period"
379 during which glucose homeostasis can be restored. We treated 14-18 week-old littermate female NOD
380 mice whose glucose levels were newly-risen above 225 mg/dL but still below 275 mg/dL with three
381 intravenous injections of 10 mg/kg peptide or Tat-only peptide control. Injections were spaced 12 hr
382 apart. 12 hr after the final injection, blood glucose was collected and flow cytometry performed on the
383 pancreas and PLNs. Strikingly, the inhibitor reversed elevated blood glucose (Fig. 7a). Control peptide
384 at the same concentration had no effect. Islet T cell infiltration and pro-inflammatory IFNγ and IL-17A
385 cytokine production were strongly reduced by JumOCA peptide treatment compared to controls (Fig.
386 7b,c). In contrast to the pancreas, PLNs showed no change in T cell numbers or percentages (Fig. 7d)

387 but similar changes in pro-inflammatory cytokine production (not shown). These data provide
388 evidence that targeting OCA-B is a valid strategy to treat emerging T1D, potentially with minimal side
389 effects, and identify a first-generation inhibitor that is efficacious in vivo.

390 **Discussion**

391 Here we show that targeting OCA-B genetically or pharmacologically can block T1D in mouse
392 models. OCA-B is a transcriptional coregulatory protein named for its strong expression in the B cell
393 lineage, where it is dispensable until after B cell activation, where it is essential for the generation of
394 germinal centers [58]. OCA-B is not expressed during thymic development or in naïve CD4 T^+ cells, but
395 is stably induced upon T^+ cell activation. In contrast, OCA-B is expressed in $CD8^+$ T cells, albeit at
396 lower levels compared to activated T cells. In both populations, OCA-B expression is maintained after
397 T cell stimulation has ceased.

398 In $CD4^+$ T cells, OCA-B associates with the POU-domain transcription factor Oct1 at ~150
399 immunomodulatory genes – among them *Il2*, *Ifng*, *Il17a* and *Csf2* (*Gmcsf*). Unlike transcription factors
400 such as NF-AT, AP-1 and NF-kB that act as primary "on" switches via direct gene activation, OCA-B
401 removes inhibitory chromatin modifications to establish permissive chromatin environments that allow
402 for silent but previously activated targets to be robustly expressed later [4, 6]. More specifically, OCA-B
403 interacts with Jmjd1a/Kdm3a, a histone lysine demethylase that removes inhibitory histone H3 lysine 9
404 methyl marks. OCA-B target gene expression is unchanged upon primary stimulation of cultured Oct1-
405 or OCA-B-deficient T cells, but upon secondary stimulation (a model of antigen reencounter) the
406 normally observed increased expression does not occur [4, 6]. In vivo, OCA-B loss leaves T cell
407 development and pathogen response unaffected, but impairs the establishment of new central memory
408 $CD4^+$ T cells. The few cells that are formed respond poorly to antigen re-encounter [4]. Repeated antigen
409 encounters that drive high levels of proinflammatory cytokines are a key feature of autoimmunity. In
410 both mice and humans, memory or memory-like cells can underlie autoimmunity including T1D [59, 60,
411 61].

412 The NOD model of T1D is spontaneous but only partially penetrant, much like the human
413 disease [62]. 60-80% of female NOD mice develop T1D in standard environments [21]. We find that
414 prediabetic OCA-B T cell deficient NOD mice harbor normal T cell numbers and similar TCR
415 specificities in their PLNs, constent with prior observations that OCA-B deficient T cells are
416 immunocompetent [4]. Nevertheless, T cell conditional OCA-B knockouts are fully protected from
417 spontaneous T1D. Protection is associated with reduced islet leukocyte infiltration and reduced
418 proinflammatory cytokine expression. Whole-body NOD *Ocab* knockouts are also protected from
419 T1D, though to a lesser degree. Prior work showed that OCA-B whole-body knockout protects mice in
420 a MOG/EAE model of multiple sclerosis [63]. In contrast, a second study showed that OCA-B whole
421 body knockout exacerbates systemic, antibody-driven autoimmunity in *Sanroque* mice [64]. The
422 protective vs. exacerbating effects in these models may be due to effects on BCR repertoire [65]. T cell-

423 specific knockout of Oct1, a transcription factor with which OCA-B docks, blocks EAE but leaves
424 responses to infection with neurotropic viruses intact [5]. Together these data indicate that in T cells
425 Oct1 and OCA-B promote autoimmunity including T1D, but that their role in B cells may be more
426 complex. OCA-B is typically expressed ~50-fold higher in B cells compared to T cells. A correctly
427 calibrated dose of competitive inhibitor could therefore be used to selectively blunt T cell-mediated
428 autoimmunity.

429 scRNAseq experiments reveal decreased neutrophil infiltration and an increase in the
430 percentage of T cells with a naïve phenotype in prediabetic OCA-B conditional knockout islets. Gene
431 expression changes were also identified that were consistent with antidiabetogenic effects of OCA-B T
432 cell knockout. For example, the remaining islet neutrophils in knockout mice show strong reductions in
433 *Cxcl2* expression compared to littermate controls. Cxcl2 is a potent neutrophil chemoattactant that
434 promotes T1D in vivo [66, 67], and therefore reductions in Cxcl2 may contribute to the reduced neutrophil
435 representation. Strikingly, OCA-B T cell deficient mice also lacked T1D-associated TCR clones in
436 their activated/memory CD8 pool. CD4 clonotypes associated with T1D were present, but associated
437 with anergy. Consistently, OCA-B loss promotes $CD4^+$ T cell anergy in vitro.

438 BDC2.5 and NY8.3 TCR transgenic mice are simplified monoclonal systems that allow easy
439 tracking of uniform T cell responses to antigens in vivo [68]. To test if OCA-B loss confers protection in
440 simplified monoclonal systems, we crossed the germline OCA-B null allele to these models, as well as
441 to RIP-mOVA transgenic mice on the C57BL/6 background. The latter mice express synthetic
442 membranous chicken ovalbumin in their thymi and pancreatic beta cells[69]. We crossed whole-body
443 null mice to the BDC2.5 transgenic line [70], which expresses a CD4-restricted TCR specific for a hybrid
444 insulin-chromogranin A peptide [71]. BDC2.5 autoreactive cells migrate to the islets and cause insulitis
445 beginning at 3-4 weeks. Due in part to Tregs that have escaped allelic exclusion, in many animals
446 insulitis is limited and does not progress to full-blown T1D. However, transferring $CD4^+CD62L^+V\beta^+$
447 or $CD4^+CD25^-$ T cells from BDC2.5 donor mice into NOD.SCID recipients results in rapid (7-10 d)
448 disease onset [34]. Transplants from both control and OCA-B null NOD/BDC2.5 mice resulted in disease
449 with similar kinetics. Identical results were also generated by depleting $CD25^+$ Tregs, or by
450 transplanting total $CD4^+$ T cells into immunodeficient NCG recipient mice. OCA-B loss also had no
451 effect using the RIP-mOVA model on the C57BL/6 background. This model expresses a synthetic
452 antigen, membranous chicken ovalbumin, in thymic epithelial and pancreatic beta cells [36].

453 In contrast to BDC2.5 and RIP-mOVA, NY8.3 transgenic mice carry a monoclonal CD8-
454 restricted TCR directed towards $IGRP_{206-214}$ and manifest spontaneous T1D [38]. Unlike BDC2.5

455 transplant models, OCA-B T cell conditional NY8.3 mice showed significant protection, though unlike
456 polyclonal NOD mice protection was incomplete. Cumulatively, the results are consistent with a model
457 in which OCA-B loss does not simply block T cell functionality, but rather desensitizes autoreactive T
458 cells. Because transgenic TCR models have fixed affinities to antigens that can be present throughout
459 disease or arise at specific points during disease etiology, they result in graded levels of disease. By
460 shifting the autoreactivity of different T cells along a spectrum of disease potentials, OCA-B loss can
461 result in full or partial protection in models with low and intermediate disease thresholds, whereas
462 models with high disease potentials remain autoreactive. Although protection in some of the more
463 severe models is likely to be inseparable from immunodeficiency, our results show that genetic
464 ablation of OCA-B strongly protects NOD animals from spontaneous T1D, and results in graded
465 protection that drops off with severity of the model. These properties make OCA-B a promising target
466 for pharmaceutical inhibition.

467 Recent work indicates that the prevailing idea that transcription regulators and protein-protein
468 interactions are "undruggable" is erroneous [47, 48, 72]. Pre-clinical membrane-penetrating peptides have
469 also been developed that successfully target transcription factors such as BCL6 [49]. We applied rational-
470 design principles to generate a membrane-permeable competitive peptide inhibitor of the interaction
471 between OCA-B and a downstream effector, Jmjd1a/Kdm3a. This inhibitor corresponds to a region of
472 the OCA-B N-terminus, which is known to include residues critical for Oct1 binding and transcription
473 activity[52]. We tested the effect of this inhibitor, termed JumOCA, on T1D onset and severity. The
474 JumOCA sequence does not coincide with other sequences in the human or mouse proteome and is not
475 predicted to be strongly immunogenic. Peptide administration into NOD mice protected animals from
476 newly-arisen T1D and significantly reduced islet-infiltrating T cell numbers and cytokine production,
477 while having more mild effects on the PLNs. OCA-B levels in B cells are at least 50-fold higher than
478 in T cells (immgen.org, [73], making it likely that the observed effects are due to inhibition in T cells.
479 The preservation of normal PLN functionality both with peptide treatment and OCA-B genetic ablation
480 suggests a potential therapeutic window in which targeting OCA-B may leave baseline immune
481 function unaffected. While these peptides are unlikely to be used in a clinical setting, they offer proof-
482 of-principle for OCA-B as a therapeutic target, and can be used as tools for the further development of
483 therapeutics.

484 **Methods**

485 **Laboratory mice.** NOD/ShiLtJ, NOD.Scid (NOD.Emv302/2.CB17-Prkdcscid), BDC-2.5 TCR
486 transgenic, NY8.3 TCR transgenic and all breeder mice were maintained in a specific pathogen-free
487 research colony. NCG (NOD-Prkdc^{em26Cd52}Il2rg^{em26Cd22}/NjuCrl) mice were purchased from Charles
488 River Laboratories. NOD.Cre^{CD4} breeding pairs were a gift from Alexander Chervonsky (University of
489 Chicago). All animal experiments were approved by the University of Utah Institutional Animal Care
490 and Use Committee (IACUC approval 17-05008).

491

492 **Generation of *Ocab* (*Pou2af1*) conditional mice.** *Pou2af1*$^{tm1a(KOMP)Wtsi}$ mice were provided by the
493 knockout mouse project (KOMP) repository (University of California, Davis). Mice were derived from
494 embryonic stem cell clone EPD0761_3_B03, generated by the Wellcome Trust Sanger Institute. These
495 cells were derived from C57BL/6N mice, but subsequent mouse crosses were to C57BL/6J (>20
496 generations) for the RIP-mOVA model and NOD (four congenic backcrosses plus an additional
497 backcross to NOD.Cre^{CD4}). The embryonic stem cells contain a CSD-targeted allele [74]. The presence of
498 WT (582 bp) and Post-FLP (700 bp) alleles was determined by PCR using CSD-Pou2af1-F and CSD-
499 Pou2af1-ttR primers. The presence of the null (801 bp) allele was determined using CSD-Pou2af1-F
500 and CSD-Pou2af1-R primers. The presence of the floxed (359 bp) allele was determined using CSD-
501 Lox-F and CSD-Pou2af1-R primers. Primer sequences were as follows: CSD-Pou2af1-F,
502 5'TACAGAGAGACTAGACACGGTCTGC; CSD-Pou2af1-R,
503 5'GATGAGGACTCTGGGTTCAGAGAGG; CSD-loxF, 5'GAGATGGCGCAACGCAATTAATG;
504 CSD-Pou2af1-ttR, 5'AGAAGGCCTCGTTACACTCCTATGC. *Ocab* conditional mice were bred with
505 mice expressing Cre under the control of the CD4 promoter.

506

507 **Backcrossing *Ocab* germline null and conditional mice to the NOD background.** To generate
508 *Ocab*$^{-/-}$ and *Ocab* conditional mice on the NOD background, the previously described C57BL/6 *Ocab*
509 germline null allele [20] and the newly-generated *Ocab* conditional allele were backcrossed to NOD
510 ShiLt/J mice using congenic markers based on Mouse Genome Informatics
511 (http://www.informatics.jax.org) (Supplementary Table 1).

512

513 **Diabetes development and assessment.** Diabetes was monitored using blood glucose test strips
514 (Contour, Bayer). Mice with blood glucose levels >250 mg/dL were considered diabetic.

515

516 **Leukocyte isolation and intracellular cytokine staining.** Pancreatic lymph nodes were grinded and
517 passed through a nylon strainer. Pancreatic leukocytes were isolated as described previously [75]. Briefly,
518 pancreata were chopped and digested using collagenase IV (1 mg/mL, Gibco) in DMEM containing
519 1% fetal bovine serum (FBS, Rocky Mountain Biologicals) and 10 units of DNase I for 15 min at
520 37°C. The digested tissues were passed through a 70 μm strainer. Red blood cells were lysed by ACK
521 (Ammonium-Chloride-Potassium) lysis buffer (150 mM NH_4Cl, 10 mM $KHCO_3$, 0.1 mM Na_2EDTA).
522 For intracellular cytokine staining, cell suspensions in RPMI medium supplemented with 10% FBS
523 were re-stimulated for 4 hr with phorbol 12-myristate 13-acetate (PMA, Sigma, 50 ng/mL) and
524 ionomycin (Sigma, 1 μg/mL) in the presence of Brefeldin-A (GolgiPlug, BD Bioscience, 1 μl/ml), and
525 fixed by cell fixation/permeabilization solution (BD Cytofix/Cytoperm) according to the
526 manufacturer's protocol. Antibodies used for flow cytometry were as follows: FITC-conjugated anti-
527 mouse CD4, PE-conjugated anti-mouse CD45, PE-conjugated anti-mouse FR4 (Biolegend), PerCP-
528 conjugated anti-mouse CD8a, APC-conjugated anti-mouse IFNγ, PE-conjugated anti-mouse IL-17,
529 PerCP-conjugated anti-mouse CD11b, APC-conjugated anti-mouse F4/80, PE-conjugated anti-mouse
530 Gr-1, PE-conjugated anti-mouse ICOS (eBioscience), PerCP-conjugated anti-mouse FoxP3, V450-
531 conjugated anti-mouse CD73 (BD Bioscience).
532
533 **T cell adoptive transfer.** 6–8 wk old NOD.Scid recipient mice were injected retro-orbitally with
534 2×10^5 of splenic $CD4^+CD25^-$ T cells from pre-diabetic *Ocab*$^{-/-}$ or *Ocab*$^{+/+}$ NOD.BDC2.5 donors (6–8
535 wk old, sex-matched). T cells were purified using a $CD4^+CD25^+$ T cell isolation kit (Miltenyi). For
536 $CD4^+CD25^+Foxp3^+$ T cells, 1.5×10^6 purified splenic $CD4^+$ T cells from pre-diabeti, BDC2.5
537 transgenic NOD.*Ocab*$^{-/-}$ or NOD.*Ocab*$^{+/+}$ mice were transferred to sex-matched 6-8 wk old NCG
538 recipients (University of Utah pre-Clinical Resource Core) as previously described [35]. For total splenic
539 transfer experiments, 5×10^6 splenocytes from pre-diabetic NOD.*Ocab*$^{fl/fl}$ or NOD.*Ocab*$^{fl/fl}$Cre^{CD4} mice
540 were transferred into sex-matched 6-8 week-old NOD.Scid recipients mice as described previously [35].
541
542 **In vivo Treg depletion.** Anti-CD25 antibody in PBS (1 mg/mouse, Clone PC61, BioXCell) was
543 administered intraperitoneally to NOD.*Ocab*$^{fl/fl}$ or NOD.*Ocab*$^{fl/fl}$Cre^{CD4} mice twice (10 and 17 d after
544 birth) as previously described [31].
545
546 **In vitro culture of CD4 T cells.** For anergic cell induction, spleens were harvested from
547 NOD.*Ocab*$^{fl/fl}$Cre^{CD4} or control NOD.*Ocab*$^{fl/fl}$ animals. Single-cell suspensions were generated by

548 grinding and passage through 70 µm strainers. $CD4^+$ T cells were isolated using a mouse $CD4^+$ T cell
549 isolation kit (Miltenyi Biotec). Isolated $CD4^+$ T cells were cultured and stimulated with 5 µg/ml plate-
550 bound anti-CD3ε (BD Bioscience) and/or 2 µg/ml anti-CD28 antibodies (eBioscience) as described
551 previously [5]. For OCA-B inhibitor peptide treatments, naïve CD4 T cells were isolated from WT
552 C57BL/6 mice using a mouse naïve $CD4^+$ T cell isolataion kit (Miltenyi Biotec) and cultured as
553 described previously [6]. For the in vitro experiments with OCA-B inhibitor peptides, indicated
554 concentrations of OCA-B inhibitor or control peptides were incubated with cells, with media changes
555 every 2 days after primary stimulation. Activation of C57BL/6 $CD4^+$ cells and subsequent profiling of
556 anergic responses was performed identifically to [5].
557
558 **Single cell RNA sequencing.** $CD3^+$ T cells were isolated from 8 week-old NOD.*Ocab*$^{fl/fl}$ or
559 NOD.*Ocab*$^{fl/fl}$Cre^{CD4} females using a pan T cell isolation kit (Miltenyi). $CD45^+$ pancreatic leukocytes
560 were isolated from 12 week-old NOD.*Ocab*$^{fl/fl}$ or NOD.*Ocab*$^{fl/fl}$Cre^{CD4} females were isolated by flow
561 cytometry using a FACS Aria instrument (Becton-Dickinson). For each condition, cells were isolated
562 from three mice and combined. Cells were processed using the 10× Genomics Chromium platform
563 according the manufacturer's instructions. Paired-end high-throughput sequencing (125 cycles) was
564 performed via an Illumina NovaSeq instrument. Sequencing reads were processed by using 10×
565 Genomics CellRanger pipeline and further analyzed using the Seurat R package. Analysis of cells used
566 a standard filtering protocol removing cells with unique feature counts of >4,000 or <500, as well as
567 cells that have >5% mitochondrial counts (indicative of dead cells). No more than 15% of total cells
568 were removed by this process.
569
570 **OCA-B mutagenesis and co-IP.** For generation of the OCA-B double point mutant, a plasmid
571 transiently expressing human OCA-B, pCATCH-Bob.1 [76], was sequentially mutagenized using
572 QuickChange (ThermoFisher). Correct mutagenesis and lack of additional mutations was confirmed by
573 resequencing. Protein expression was confirmed by transiently transfect HCT116 cells, which do not
574 express endogenous OCA-B. HCT116 lysate preparation, co-immunoprecipitation of OCA-B and
575 endogenous Jmjd1a, and immunoblot detection was performed using the same conditions as described
576 [4]. For co-IP using M12 cells, lysis buffer consisted of 50 mM Tris-Cl, pH 7.4, 150mM NaCl, 0.5%NP-
577 40, 1 mM EDTA,1 mM EGTA, plus protease/phosphatase inhibitors (PhosSTOP, Roche). Lysates
578 were incubated with 2.5 µg Jmjd1A antibody (Bethyl) and protein-G Dynabeads (ThermoFisher) in
579 lysis buffer containing 20% glycerol overnight at 4°C. After overnight incubation, the indicated

580 concentrations of peptide or PBS vehicle was added and incubated for a further 3 hr at 4°C prior to
581 bead precipitation and washing 3× in lysis buffer plus 20% glycerol. Co-precipitated OCA-B was
582 analyzed by SDS-PAGE and immunoblot.
583
584 **OCA-B inhibitor peptide synthesis.** Unique chemically synthesized peptide sequences were as
585 follows: Peptide#1, ARPYQGVRVKEPVK; Peptide#2/JumOCA, VKELLRRKRGH; Peptide#3,
586 ARPYQGVRVKEPVKELLRRKRGH; Scrambled peptide, VLREKGKRHLR. Peptides were
587 synthesized with and without a covalent C-terminal linker and Tat membrane-penetrating peptide
588 (GSG-GRKKRRQRRRGY). Fmoc protected amino acids were obtained from Protein Technologies
589 Inc. 1-[Bis(dimethylamino)methylene]-1H-1,2,3-triazolo[4,5-b]pyridinium 3-oxid
590 hexafluorophosphate (HATU) was purchased from Chemimpex Inc. H-Rink-Amide-ChemMatrix
591 (RAM) was purchased from Biotage. N,N-diisopropylethylamine (DIEA), dichloromethane (DCM),
592 triisopropylsilane (TIS) were purchased from Sigma Aldrich. Dimethylformamide (DMF),
593 trifluoroacetic acid (TFA), acetonitrile (ACN), and ethyl ether were purchased from Fisher Scientific.
594 Peptides were synthesized using automated Fmoc SPPS chemistry on synthesizer (Syro I). Briefly, 220
595 mg of RAM resin (Loading = 0.45 mmol/g) was swelled in DCM for 15 min and followed by adding in
596 a solution of specific Fmoc protected amino acid (AA = 0.1 mmol, DIEA = 0.2 mmol in DCM = 4 mL)
597 and incubated at room temperature for 1.5 h. Then the resin was washed with DMF and DCM and
598 incubated with 5 mL of DCM containing 16% v/v MeOH and 8% v/v DIEA for 5 min. This action was
599 repeated for 5 times before thoroughly washed with DCM and DMF. Then the resin was set to
600 synthesizer for automated synthesis. Coupling reactions were performed using HATU (5 eq.), DIPEA
601 (10 eq.) and amino acid (5 eq.) in DMF with 15 min heating to 70 oC (50 oC for Cys). Deprotection
602 reaction was performed using 20% (v/v) Piperidine in DMF, 5 min rt for 2 rounds. Peptides were
603 cleaved from the resin by treatment with a cocktail buffer (3 mL/0.1 mmol, TFA:H2O:TIS:EDT =
604 95:2:2:1) for 2.5 h. Peptide-TFA solution was then filtered and precipitated in cold ether, and
605 centrifuged and washed with ether twice and vacuum-dried. The crude product was then purified by
606 RP HPLC. Peptides characterization was performed by LC/MS on an Xbridge C18 5 µm (50 x 2.1
607 mm) column at 0.4 mL/min with a water/acetonitrile gradient in 0.1% formic acid on an Agilent 6120
608 Quadrupole LC/MS system. Fractions collected from HPLC runs were also analyzed by LC/MS. The
609 purified fractions containing the targeted product were collected and lyophilized using a Labconco
610 Freeze Dryer. All samples were analyzed by the following conditions: Preparative reverse phase HPLC
611 of crude peptides was performed on a Jupiter 5 µ C18 300 Å (250×10 mm) column at 3 mL/min with a
612 water/acetonitrile (ACN) gradient in 0.1% TFA on an Agilent 1260 HPLC system. Purity, isomer co-

613 injection and stability checks were performed on HPLC on Phenomenex Gemini C18 3 µm (110 Å
614 150×3 mm) column.
615
616 **OCA-B inhibitor peptide treatment.** Anesthetized pre-diabetic WT NOD females with glucose levels
617 newly-risen to between 225 to 275 mg/dL were treated with the inhibitor or control peptides by
618 intravenous (retro-orbital) injection, 3 times every 12 hr. Blood glucose levels were measured at every
619 injection. 4 hr after the last injection, pancreata and pancreatic lymph nodes (PLNs) were collected and
620 cell populations were analyzed by flow cytometry.
621
622 **Histology.** Formalin-fixed pancreatic tissues were embedded in paraffin. Sections were IHC-stained or
623 H&E-strained. The slides were developed with DAB peroxidase substrate. IHC antibodies were as
624 follows: XXXX, YYYYY, ZZZZZ. Islet inflammation was scored as follows based on published
625 precedents [77]: 1, no insulitis; 2, peri-insulitis (inflammatory cells in the immediate vicinity of the
626 islets); 3, insulitis (a clear infiltration of inflammatory cells in islet that are directly around β cell).
627 Frozen pancreatic sections were XXXXX YYYYY ZZZZZ.
628
629 **Statistical analyses.** All error bars denote ± SEM. Two-tailed student T-tests were used to ascribe
630 statistical significance. For all figures, *=*p*-value ≤0.05; **=*p*-value ≤0.01.

Acknowledgements

We thank P. Santamaria and F. Gounari for critical reading of the manuscript. We thank A. Chervonsky (U. Chicago) for the gift of NOD.Cre^{CD4} mice. We thank J. Marvin and the University of Utah Health Sciences Center Flow Cytometry Core facility for assistance with flow cytometry. We thank M. Hanson and the University of Utah Health Sciences DNA/peptide synthesis core. This work was supported by grants to DT from the Praespero Foundation, Juvenille Diabetes Research Foundation (1-INO-2018-647-A-N) and National Institutes of Health (R01-AI100873).

Author's contributions

DT conceived the study and designed experiments, supervised the study, and provided administrative, technical and material support. HK, AS, AI and JLJ acquired and interpreted the data. JP performed high-level analysis of scRNAseq and TCR clonotype data. CG helped generate critical reagents. BDE, DH-CC, XH and PJ provided material and intellectual support. All authors were involved in writing, reviewing and revising the manuscript.

645 **Figure legends**

646

647 **Fig. 1 | Loss of OCA-B protects NOD mice from T1D. a**, Targeting event. Crossing with ROSA-FLP
648 results in conditional (*fl*) allele. Primer-pairs used for genotyping are depicted with arrows. **b**, Example
649 genotyping of the targeted allele and recombination events. Founder animal is in lane 2. The primer-
650 pairs shown in (a) were used. **c**, The *Ocab* (*Pou2af1*) conditional allele was crossed to Cre^{CD4}. Total
651 splenic $CD4^+$ T cells were isolated from an $Ocab^{fl/fl}Cre^{CD4}$ animal or a $Ocab^{+/fl}Cre^{CD4}$ littermate
652 control, and stimulated for 2 d in vitro using plate-bound CD3ε and soluble CD28 antibodies. An
653 OCA-B immunoblot of stimulated total T cells is shown. β-actin is shown as a loading control. **d**,
654 Kaplan-Meier plot of diabetes-free survival in littermate female NOD.$Ocab1^{fl/fl}Cre^{CD4}$ (n=12) and
655 NOD.$Ocab1^{fl/fl}$ (n=14) mice. Diabetes criterion was ≥250 mg/dL blood glucose. **e**, Avearage blood
656 glucose levels from mice shown in panel (c) is shown. **f**, Mean glucose levels from panel (d) at
657 endpoint (24 weeks of age). *P*=0.0402. **g**, Percent diabetes-free survival in germline knockout
658 NOD.$Ocab^{-/-}$ (n=16) and control NOD.$Ocab^{+/+}$ (n=17) mice were plotted based blood glucose cutoff of
659 ≥250 mg/dL.

660

661 **Fig. 2 | NOD.*Ocab* conditional mice have fewer islet IFNγ expressing CD8 T cells and**
662 **macrophages, and more Tregs compared to controls. a**, Pancreatic islet leukocytes were isolated
663 from 8 week- or 24 week-old littermate female NOD.$Ocab1^{fl/fl}Cre^{CD4}$ (8 week; n=3, 24 week; n=5) or
664 NOD.$Ocab1^{fl/fl}$ (8 week; n=3, 24 week; n=4) mice and analyzed by flow cytometry. Mean
665 $CD45^+CD11b^+F4/80^+$ cell frequencies are depicted. **b**, Frequencies of $CD45^+CD11b^+F4/80^+$ cells from
666 representative animals in panel (a) are shown. Plots were gated on $CD45^+$ cells. **c**, Mean percentages of
667 total pancreatic-infiltrating $CD8^+$ T cell in 12 week-old NOD.$Ocab1^{fl/fl}Cre^{CD4}$ or control
668 NOD.$Ocab1^{fl/fl}$ mice are plotted. Cells were independently purified from 3 pancreata and gated on
669 $CD45^+$. **d**, IFNγ expressing $CD8^+$ T cell percentages in 16 week old-NOD.$Ocab1^{fl/fl}Cre^{CD4}$ (n=3) and
670 littermate control islets (n=5) are shown. **e**, Percentages of FoxP3-expressing $CD4^+$ T cells in pre-
671 diabetic (8 week) NOD.*Ocab* conditional and control female mice are plotted. N=3 for each group.
672 Mean of results is shown. **f**, NOD.$Ocab^{fl/fl}$ or NOD.$Ocab^{fl/fl}Cre^{CD4}$ pups were treated with anti-CD25
673 antibodies intraperitoneally on day 10 and 17 after birth to depleted Tregs. Mice were monitored for
674 T1D emergence as in Fig. 1.

675

676 **Fig. 3 | T cell conditional OCA-B loss reduces the numbers of activated, autoreactive pancreatic**
677 **islet T cells. a**, scRNAseq was performed using total islet $CD45^+$ cells from prediabetic
678 NOD.*Ocab*$^{fl/fl}$Cre^{CD4} or control NOD.*Ocab*$^{fl/fl}$ mice (n=3 for each group). Cell populations were plotted
679 using UMAP (Seurat R package) and percentages in each cluster are shown for each genotype.
680 Different populations were identified using Seurat R package function FindMarkers. **b**, Four
681 populations from panel (a) were analyzed for differential gene expression. Identified genes are shown
682 as a scatter plot. Significantly differentially expressed genes (adjusted *p*-value <0.05) are shown in red.
683 **c**, UMAP plots similar to (a) are shown, except cells expressing TCR clonotype 13-3 are shown. The
684 non-naïve (activated+memory) $CD8^+$ cell population identified in (a) is shown in red. **d**, Percent
685 contribution of the top 21 identified TCR clonotypes to total activated+memory $CD8^+$ cells is shown.
686 The V genes comprising the top 6 clonotypes are also shown. **e**, Cells positive for clonotypes 1-5 are
687 shown for two clusters, non-naïve (activated+memory) $CD8^+$ T cells and $CTLA4^+FR4^+$ anergic cells
688 (consisting of mostly $CD4^+$ cells). For each cluster, positive cells are shown in dark blue. An overlay
689 of control and OCA-B deficient cell populations is shown, however because each clonotype is only
690 observed in a single genotype (panel d), all cells can be mapped back entirely to OCA-B deficient or
691 control (clonotypes 1 and 4: OCA-B deficient; clonotypes 2, 3 and 5: control).
692
693 **Fig. 4 | OCA-B loss protects NOD mice from T1D in spontaneous and polyclonal splenocyte**
694 **transfer models but not in models using transfer of monoclonal autoreactive T cells. a**, 2×10^5
695 purified $CD4^+CD25^-$ splenic T cells from NOD.BDC2.5.*Ocab*$^{-/-}$ or control NOD.BDC2.5.*Ocab*$^{+/+}$
696 donors were injected retro-orbitally into NOD.Scid (n=6 for each group) mice. Diabetes-free survival
697 (≥250 mg/dL) is shown. **b**, 1.5×10^6 purified splenic total $CD4^+$ T cells from NOD.BDC2.5.*Ocab*$^{-/-}$ or
698 control donors were transferred into NCG mice (n=5 for each group). Mice were monitored for
699 diabetes development. **c**, Total NOD splenocytes (5×10^6) from prediabetic 6- to 8-wk-old sex-matched
700 NOD.*Ocab1*$^{fl/fl}$Cre^{CD4} or control NOD.*Ocab1*$^{fl/fl}$ donors were adoptively transferred into sex-matched
701 NOD.Scid (n=7 for each group) recipients. Diabetes incidence rates are shown. **d**, At 13 weeks post-
702 transfer, the proportion of IFNγ-expressing $CD8^+$ T cells was assessed by flow cytometry in pancreata
703 isolated from mice receiving splenocytes from NOD.*Ocab1*$^{fl/fl}$Cre^{CD4} or NOD.*Ocab1*$^{fl/fl}$ donors in panel
704 (c). **e**, The Ocab null allele was crossed to NY8.3 TCR transgenic mice. Spontaneous T1D was
705 measured in female *Ocab*$^{-/-}$ or control *Ocab*$^{+/+}$ littermates (n=XX for each group). **f**, Naïve $CD4^+$ or
706 $CD8^+$ T cells were isolated from C57BL/6 spleens and stimulated for up to two days in vitro using
707 anti-CD3ε and CD28 antibodies. Cells were then washed and replated in the presence of exogenous IL-

708 2. After 8 days rest in culture, cells were restimulated for 6 hr. Lysates were prepared from each step
709 and subjected to OCA-B immunoblotting to assess changes in expression. Oct1 and β-actin are shown
710 as controls.
711
712 **Fig. 5 | OCA-B loss in CD4$^+$ T cells increases anergy in vitro. a**, Naïve OCA-B deficient and control
713 CD4$^+$ T cells were stimulated in vitro with anti-CD3ε antibodies. 48 hr later, the cells were re-
714 stimulated with PMA and ionomycin, and analyzed by flow cytometry. Representative frequencies of
715 cytokine expressing CD4$^+$ CD44$^+$ cells are shown. **b**, Quantitatition using independently purified cells
716 from the spleens of 4 mice treated similar to (a). **c**, OCA-B deficient and control CD4$^+$ T cells were
717 stimulated in vitro with indicated antibodies, and analyzed by flow cytometry. Mean of FR4^{hi} CD73^{hi}
718 CD4$^+$ CD44$^+$ cell frequencies are shown using independently purified cells from the spleens of 3 mice,
719 with two technical culture replicates performed for each mouse (n=6). **d**, Similar to panel (c), except
720 frequencies of CD4$^+$CD44$^+$ICOS$^+$ cells are plotted. **e**, Similar to panel (c), except average percentage
721 of CD4$^+$CD44$^+$CD25$^+$ cells are plotted.
722
723 **Fig. 6 | Design and validation of OCA-B peptide inhibitors. a**, OCA-B N-terminus/Oct1 DNA
724 binding domain/octamer binding DNA co-crystal structure (PDB ID 1CQT)[48]. Gray: DNA. Green:
725 Oct1 DNA binding domain. Cyan: OCA-B. Structured OCA-B N- and C-termini (residues 16 and 38)
726 are labeled. Relevant OCA-B residues from panel (b) are highlighted. Red dashed line shows position
727 of the Oct1 linker domain. **b**, Top alignment of the human androgen receptor (AR) isoform transcript
728 variant 1 (Sequence ID: ADD26780.1) co-activator interaction domain (residues 698-721) with full-
729 length human Oct1 and OCA-B. The Oct1 linker domain and OCA-B N-terminus most resemble the
730 area of AR that interacts with Jmjd1a. Green serines: putative ERK phospho-acceptor sites. Yellow:
731 similar or identical amino acids. Asterisks: known human point mutations that block coactivator
732 binding and cause androgen insensitivity syndrome in humans. Pairwise alignments were performed
733 using the FASTA algorithm (https://embnet.vital-it.ch/software/LALIGN_form.html) and trimmed for
734 the 3-way overlap. **c**, Alignment of human and mouse primary OCA-B peptide sequences. **d**, Co-IP of
735 Jmjd1a with double point-mutant OCA-B and wild-type control. HCT116 cells (which lack
736 endogenous OCA-B) transfected with WT or mutant OCA-B constructs were used. Expression of
737 proteins was checked 48 hrs after transfection by Western blotting. 50 μg protein was loaded in each
738 lane. **e**, Indicated peptide sequences were synthesized as C-terminal Tat fusions for membrane
739 permeability. Arrows indicate position of mutant in (b) and (d). **f**, *Il2* mRNA expression in primary

740 $CD4^+$ T cells treated with 50 μM JumOCA peptide was measured relative to β-actin internal standard
741 by RT-qPCR. Cells were stimulated with CD3ε/CD28 antibodies for two days, rested for a further 8
742 days in the presence of exogenous recombinant IL-2, and restimulated for a further 6 hr. Peptide was
743 included during resting and restimulation only, and replaced every other day with media changes. **g**,
744 IL-2 cytokine expression in primary $CD4^+$ T cells cultured with 50μM peptide at initial treatment, and
745 with 25μM peptide from the secondary treatment was measured by flow cytometry. Cells were treated
746 similarly to (f) except collection, brefeldin A treatment and processing for flow cytometry occurred 24
747 hr post-restimulation. **h**, $CD4^+CD44^+IL2^+$ T cell frequencies from representative samples in panel (g)
748 are shown. Plots were gated on CD4 and CD44. **i**, The interaction between OCA-B and Jmjd1a was
749 measured in a co-immunoprecipitation assay. After incubation with protein-G beads, the indicated
750 amounts of peptide or vehicle control were added for a further 3 hr prior to precipitation and washing.
751 1% input (lane 1) is shown as a control.
752
753 **Fig. 7 | OCA-B inhibitor peptide injections protect NOD mice from newly-arisen diabetes. a**, 3
754 doses of 10 mg/kg OCA-B inhibitor peptide (n=4) or control peptide (n=5) were injected retro-orbitally
755 every 12 hr into 12-18 week-old NOD female littermate mice whose glucose levels were newly-risen
756 above 225 mg/dL but still below 275 mg/dL. Glucose levels of peptide injected mice are shown right
757 before each injection, and 12 hr after final injection. Control peptide=Tat alone. **b**, 4hr after the last
758 injection of peptides in panel (a), PLN $CD4^+$ and $CD8^+$ T cell percentagess were analyzed by flow
759 cytometry. **c**, Mean of islet IL-17 expressing T cells in the same mice as in (b) were analyled by flow
760 cytometry and plotted. **d**, Similar analysis as (c) except for IFNγ.
761

762 **References**

763 1. Lernmark, A. & Larsson, H.E. Immune therapy in type 1 diabetes mellitus. *Nat Rev Endocrinol* **9**, 92-
764 103 (2013).

765 2. Cooke, D.W. & Plotnick, L. Type 1 diabetes mellitus in pediatrics. *Pediatr Rev* **29**, 374-384; quiz 385
766 (2008).

767 3. Staeva, T.P., Chatenoud, L., Insel, R. & Atkinson, M.A. Recent lessons learned from prevention and
768 recent-onset type 1 diabetes immunotherapy trials. *Diabetes* **62**, 9-17 (2013).

769 4. Shakya, A. *et al.* Oct1 and OCA-B are selectively required for CD4 memory T cell function. *J Exp Med*
770 **212**, 2115-2131 (2015).

771 5. Kim, H. *et al.* T cell-selective deletion of Oct1 protects animals from autoimmune neuroinflammation
772 while maintaining neurotropic pathogen response. *J Neuroinflammation* **16**, 133 (2019).

773 6. Shakya, A., Kang, J., Chumley, J., Williams, M.A. & Tantin, D. Oct1 is a switchable, bipotential
774 stabilizer of repressed and inducible transcriptional states. *The Journal of biological chemistry* **286**, 450-
775 459 (2011).

776 7. Yosef, N. *et al.* Dynamic regulatory network controlling TH17 cell differentiation. *Nature* **496**, 461-468
777 (2013).

778 8. van Heel, D.A. *et al.* Inflammatory bowel disease is associated with a TNF polymorphism that affects
779 an interaction between the OCT1 and NF(-kappa)B transcription factors. *Hum Mol Genet* **11**, 1281-1289
780 (2002).

781 9. Vince, N. *et al.* HLA-C Level Is Regulated by a Polymorphic Oct1 Binding Site in the HLA-C Promoter
782 Region. *Am J Hum Genet* **99**, 1353-1358 (2016).

783 10. Cunninghame Graham, D.S., Wong, A.K., McHugh, N.J., Whittaker, J.C. & Vyse, T.J. Evidence for
784 unique association signals in SLE at the CD28-CTLA4-ICOS locus in a family-based study. *Hum Mol*
785 *Genet* **15**, 3195-3205 (2006).

786 11. Kiesler, P., Shakya, A., Tantin, D. & Vercelli, D. An allergy-associated polymorphism in a novel
787 regulatory element enhances IL13 expression. *Hum Mol Genet* **18**, 4513-4520 (2009).

788 12. Farh, K.K. *et al.* Genetic and epigenetic fine mapping of causal autoimmune disease variants. *Nature*
789 **518**, 337-343 (2015).

790 13. Maurano, M.T. *et al.* Systematic localization of common disease-associated variation in regulatory
791 DNA. *Science* **337**, 1190-1195 (2012).

792 14. Leon Rodriguez, D.A., Carmona, F.D., Echeverria, L.E., Gonzalez, C.I. & Martin, J. IL18 Gene
793 Variants Influence the Susceptibility to Chagas Disease. *PLoS Negl Trop Dis* **10**, e0004583 (2016).

794 15. Games Collaborative, G. *et al.* Linkage disequilibrium screening for multiple sclerosis implicates JAG1
795 and POU2AF1 as susceptibility genes in Europeans. *J Neuroimmunol* **179**, 108-116 (2006).

796 16. Nakamura, M. *et al.* Genome-wide association study identifies TNFSF15 and POU2AF1 as
797 susceptibility loci for primary biliary cirrhosis in the Japanese population. *Am J Hum Genet* **91**, 721-728
798 (2012).

799 17. Serreze, D.V. *et al.* B lymphocytes are essential for the initiation of T cell-mediated autoimmune
800 diabetes: analysis of a new "speed congenic" stock of NOD.Ig mu null mice. *J Exp Med* **184**, 2049-2053
801 (1996).

802 18. Hattori, M. *et al.* The NOD mouse: recessive diabetogenic gene in the major histocompatibility
803 complex. *Science* **231**, 733-735 (1986).

804 19. Serreze, D.V. *et al.* Subcongenic analysis of the Idd13 locus in NOD/Lt mice: evidence for several
805 susceptibility genes including a possible diabetogenic role for beta 2-microglobulin. *J Immunol* **160**,
806 1472-1478 (1998).

807 20. Kim, U. *et al.* The B-cell-specific transcription coactivator OCA-B/OBF-1/Bob-1 is essential for normal
808 production of immunoglobulin isotypes. *Nature* **383**, 542-547 (1996).

809 21. Makino, S., Muraoka, Y., Kishimoto, Y. & Hayashi, Y. Genetic analysis for insulitis in NOD mice.
810 *Jikken Dobutsu* **34**, 425-431 (1985).

811 22. Rosmalen, J.G. *et al.* Subsets of macrophages and dendritic cells in nonobese diabetic mouse pancreatic
812 inflammatory infiltrates: correlation with the development of diabetes. *Lab Invest* **80**, 23-30 (2000).

813 23. Peterson, J.D., Berg, R., Piganelli, J.D., Poulin, M. & Haskins, K. Analysis of leukocytes recruited to
814 the pancreas by diabetogenic T cell clones. *Cell Immunol* **189**, 92-98 (1998).

815 24. Cantor, J. & Haskins, K. Recruitment and activation of macrophages by pathogenic CD4 T cells in type
816 1 diabetes: evidence for involvement of CCR8 and CCL1. *J Immunol* **179**, 5760-5767 (2007).

817 25. Schloot, N.C. *et al.* Serum IFN-gamma and IL-10 levels are associated with disease progression in non-
818 obese diabetic mice. *Diabetes Metab Res Rev* **18**, 64-70 (2002).

819 26. Newby, B.N. *et al.* Type 1 Interferons Potentiate Human CD8(+) T-Cell Cytotoxicity Through a
820 STAT4- and Granzyme B-Dependent Pathway. *Diabetes* **66**, 3061-3071 (2017).

821 27. Krishnamurthy, B. *et al.* Autoimmunity to both proinsulin and IGRP is required for diabetes in
822 nonobese diabetic 8.3 TCR transgenic mice. *J Immunol* **180**, 4458-4464 (2008).

823 28. Wang, B. *et al.* Interferon-gamma impacts at multiple points during the progression of autoimmune
824 diabetes. *Proc Natl Acad Sci U S A* **94**, 13844-13849 (1997).

825 29. Brode, S., Raine, T., Zaccone, P. & Cooke, A. Cyclophosphamide-induced type-1 diabetes in the NOD
826 mouse is associated with a reduction of CD4+CD25+Foxp3+ regulatory T cells. *J Immunol* **177**, 6603-
827 6612 (2006).

828 30. Jaeckel, E., von Boehmer, H. & Manns, M.P. Antigen-specific FoxP3-transduced T-cells can control
829 established type 1 diabetes. *Diabetes* **54**, 306-310 (2005).

830 31. Mellanby, R.J., Thomas, D., Phillips, J.M. & Cooke, A. Diabetes in non-obese diabetic mice is not
831 associated with quantitative changes in CD4+ CD25+ Foxp3+ regulatory T cells. *Immunology* **121**, 15-
832 28 (2007).

833 32. Wong, C.P., Li, L., Frelinger, J.A. & Tisch, R. Early autoimmune destruction of islet grafts is associated
834 with a restricted repertoire of IGRP-specific CD8+ T cells in diabetic nonobese diabetic mice. *J*
835 *Immunol* **176**, 1637-1644 (2006).

836 33. Li, L. *et al.* beta cell-specific CD4+ T cell clonotypes in peripheral blood and the pancreatic islets are
837 distinct. *J Immunol* **183**, 7585-7591 (2009).

838 34. Berry, G. & Waldner, H. Accelerated type 1 diabetes induction in mice by adoptive transfer of
839 diabetogenic CD4+ T cells. *J Vis Exp*, e50389 (2013).

840 35. Presa, M. *et al.* The Presence and Preferential Activation of Regulatory T Cells Diminish Adoptive
841 Transfer of Autoimmune Diabetes by Polyclonal Nonobese Diabetic (NOD) T Cell Effectors into NSG
842 versus NOD-scid Mice. *J Immunol* **195**, 3011-3019 (2015).

843 36. Van Belle, T.L., Taylor, P. & von Herrath, M.G. Mouse Models for Type 1 Diabetes. *Drug Discov*
844 *Today Dis Models* **6**, 41-45 (2009).

845 37. Kurts, C. *et al.* CD4+ T cell help impairs CD8+ T cell deletion induced by cross-presentation of self-
846 antigens and favors autoimmunity. *J Exp Med* **186**, 2057-2062 (1997).

847 38. Verdaguer, J. *et al.* Spontaneous autoimmune diabetes in monoclonal T cell nonobese diabetic mice. *J*
848 *Exp Med* **186**, 1663-1676 (1997).

849 39. Kalekar, L.A. *et al.* CD4(+) T cell anergy prevents autoimmunity and generates regulatory T cell
850 precursors. *Nat Immunol* **17**, 304-314 (2016).

851 40. Vanasek, T.L., Khoruts, A., Zell, T. & Mueller, D.L. Antagonistic roles for CTLA-4 and the
852 mammalian target of rapamycin in the regulation of clonal anergy: enhanced cell cycle progression
853 promotes recall antigen responsiveness. *J Immunol* **167**, 5636-5644 (2001).

854 41. Kearney, E.R., Pape, K.A., Loh, D.Y. & Jenkins, M.K. Visualization of peptide-specific T cell
855 immunity and peripheral tolerance induction in vivo. *Immunity* **1**, 327-339 (1994).

856 42. Chai, J.G. & Lechler, R.I. Immobilized anti-CD3 mAb induces anergy in murine naive and memory
857 CD4+ T cells in vitro. *Int Immunol* **9**, 935-944 (1997).

858 43. Tuettenberg, A. *et al.* The role of ICOS in directing T cell responses: ICOS-dependent induction of T
859 cell anergy by tolerogenic dendritic cells. *J Immunol* **182**, 3349-3356 (2009).

860 44. Dong, C. & Nurieva, R.I. Regulation of immune and autoimmune responses by ICOS. *J Autoimmun* **21**,
861 255-260 (2003).

862 45. Dong, C. *et al.* ICOS co-stimulatory receptor is essential for T-cell activation and function. *Nature* **409**,
863 97-101 (2001).

864 46. Martinez, R.J. *et al.* Arthritogenic self-reactive CD4+ T cells acquire an FR4hiCD73hi anergic state in
865 the presence of Foxp3+ regulatory T cells. *J Immunol* **188**, 170-181 (2012).

866 47. Skwarczynska, M. & Ottmann, C. Protein-protein interactions as drug targets. *Future Med Chem* **7**,
867 2195-2219 (2015).

868 48. Green, D.R. A BH3 Mimetic for Killing Cancer Cells. *Cell* **165**, 1560 (2016).

869 49. Polo, J.M. *et al.* Specific peptide interference reveals BCL6 transcriptional and oncogenic mechanisms
870 in B-cell lymphoma cells. *Nat Med* **10**, 1329-1335 (2004).

871 50. Chasman, D., Cepek, K., Sharp, P.A. & Pabo, C.O. Crystal structure of an OCA-B peptide bound to an
872 Oct-1 POU domain/octamer DNA complex: specific recognition of a protein-DNA interface. *Genes Dev*
873 **13**, 2650-2657 (1999).

874 51. Klemm, J.D., Rould, M.A., Aurora, R., Herr, W. & Pabo, C.O. Crystal structure of the Oct-1 POU
875 domain bound to an octamer site: DNA recognition with tethered DNA-binding modules. *Cell* **77**, 21-32
876 (1994).

877 52. Gstaiger, M., Georgiev, O., van Leeuwen, H., van der Vliet, P. & Schaffner, W. The B cell coactivator
878 Bob1 shows DNA sequence-dependent complex formation with Oct-1/Oct-2 factors, leading to
879 differential promoter activation. *EMBO J* **15**, 2781-2790 (1996).

880 53. Yamane, K. *et al.* JHDM2A, a JmjC-containing H3K9 demethylase, facilitates transcription activation
881 by androgen receptor. *Cell* **125**, 483-495 (2006).

882 54. Thin, T.H. *et al.* Mutations in the helix 3 region of the androgen receptor abrogate ARA70 promotion of
883 17beta-estradiol-induced androgen receptor transactivation. *The Journal of biological chemistry* **277**,
884 36499-36508 (2002).

885 55. Schwarze, S.R., Hruska, K.A. & Dowdy, S.F. Protein transduction: unrestricted delivery into all cells?
886 *Trends Cell Biol* **10**, 290-295 (2000).

887 56. Caron, N.J., Quenneville, S.P. & Tremblay, J.P. Endosome disruption enhances the functional nuclear
888 delivery of Tat-fusion proteins. *Biochem Biophys Res Commun* **319**, 12-20 (2004).

889 57. Krautwald, S., Ziegler, E., Tiede, K., Pust, R. & Kunzendorf, U. Transduction of the TAT-FLIP fusion
890 protein results in transient resistance to Fas-induced apoptosis in vivo. *The Journal of biological*
891 *chemistry* **279**, 44005-44011 (2004).

892 58. Shi, W. *et al.* Transcriptional profiling of mouse B cell terminal differentiation defines a signature for
893 antibody-secreting plasma cells. *Nat Immunol* **16**, 663-673 (2015).

894 59. Kawakami, N. *et al.* Autoimmune CD4+ T cell memory: lifelong persistence of encephalitogenic T cell
895 clones in healthy immune repertoires. *J Immunol* **175**, 69-81 (2005).

896 60. Yeo, L. *et al.* Autoreactive T effector memory differentiation mirrors beta cell function in type 1
897 diabetes. *J Clin Invest* **128**, 3460-3474 (2018).

898 61. Chee, J. *et al.* Effector-memory T cells develop in islets and report islet pathology in type 1 diabetes. *J*
899 *Immunol* **192**, 572-580 (2014).

900 62. Parker, M.J. *et al.* Immune depletion with cellular mobilization imparts immunoregulation and reverses
901 autoimmune diabetes in nonobese diabetic mice. *Diabetes* **58**, 2277-2284 (2009).

902 63. Ikegami, I., Takaki, H., Kamiya, S., Kamekura, R. & Ichimiya, S. Bob1 enhances RORgammat-
903 mediated IL-17A expression in Th17cells through interaction with RORgammat. *Biochem Biophys Res*
904 *Commun* **514**, 1167-1171 (2019).

905 64. Chevrier, S., Kratina, T., Emslie, D., Karnowski, A. & Corcoran, L.M. Germinal center-independent,
906 IgM-mediated autoimmunity in sanroque mice lacking Obf1. *Immunol Cell Biol* **92**, 12-19 (2014).

907 65. Casellas, R. *et al.* OcaB is required for normal transcription and V(D)J recombination of a subset of
908 immunoglobulin kappa genes. *Cell* **110**, 575-585 (2002).

909 66. Citro, A. *et al.* CXCR1/2 inhibition blocks and reverses type 1 diabetes in mice. *Diabetes* **64**, 1329-1340
910 (2015).

911 67. Diana, J. & Lehuen, A. Macrophages and beta-cells are responsible for CXCR2-mediated neutrophil
912 infiltration of the pancreas during autoimmune diabetes. *EMBO Mol Med* **6**, 1090-1104 (2014).

913 68. Haskins, K. Pathogenic T-cell clones in autoimmune diabetes: more lessons from the NOD mouse. *Adv*
914 *Immunol* **87**, 123-162 (2005).

915 69. Kurts, C. *et al.* Constitutive class I-restricted exogenous presentation of self antigens in vivo. *J Exp Med*
916 **184**, 923-930 (1996).

917 70. Katz, J.D., Wang, B., Haskins, K., Benoist, C. & Mathis, D. Following a diabetogenic T cell from
918 genesis through pathogenesis. *Cell* **74**, 1089-1100 (1993).

919 71. Delong, T. *et al.* Pathogenic CD4 T cells in type 1 diabetes recognize epitopes formed by peptide
920 fusion. *Science* **351**, 711-714 (2016).

921 72. Zuber, J. *et al.* RNAi screen identifies Brd4 as a therapeutic target in acute myeloid leukaemia. *Nature*
922 **478**, 524-528 (2011).

923 73. Zwilling, S., Dieckmann, A., Pfisterer, P., Angel, P. & Wirth, T. Inducible expression and
924 phosphorylation of coactivator BOB.1/OBF.1 in T cells. *Science* **277**, 221-225 (1997).

925 74. Testa, G. *et al.* A reliable lacZ expression reporter cassette for multipurpose, knockout-first alleles.
926 *Genesis* **38**, 151-158 (2004).

927 75. Sitrin, J., Ring, A., Garcia, K.C., Benoist, C. & Mathis, D. Regulatory T cells control NK cells in an
928 insulitic lesion by depriving them of IL-2. *J Exp Med* **210**, 1153-1165 (2013).

929 76. Gstaiger, M., Knoepfel, L., Georgiev, O., Schaffner, W. & Hovens, C.M. A B-cell coactivator of
930 octamer-binding transcription factors. *Nature* **373**, 360-362 (1995).

931 77. Zhang, C. *et al.* Elimination of insulitis and augmentation of islet beta cell regeneration via induction of
932 chimerism in overtly diabetic NOD mice. *Proc Natl Acad Sci U S A* **104**, 2337-2342 (2007).

933

934

Kim et al. Figure 1

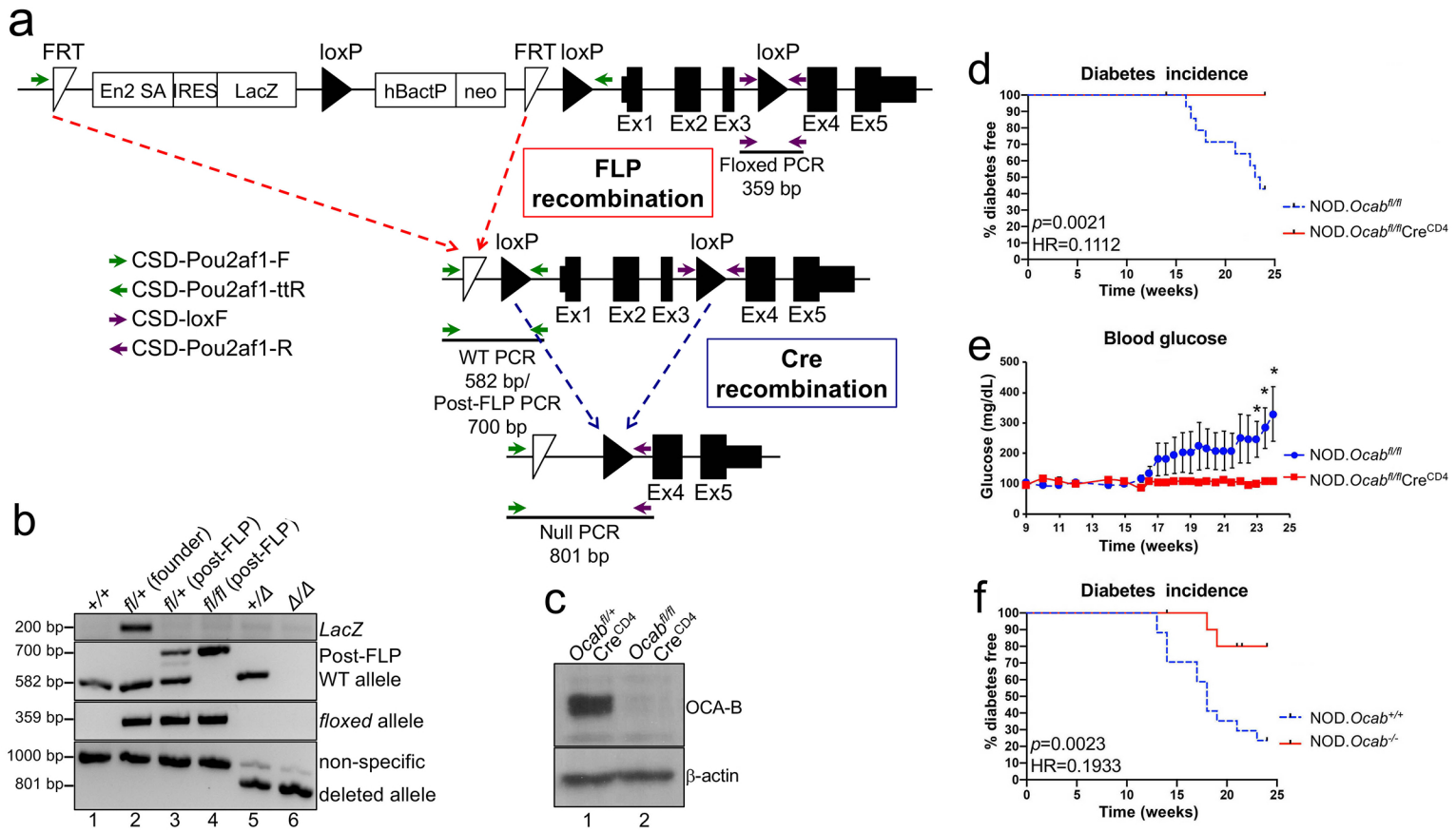

Kim et al. Figure 2

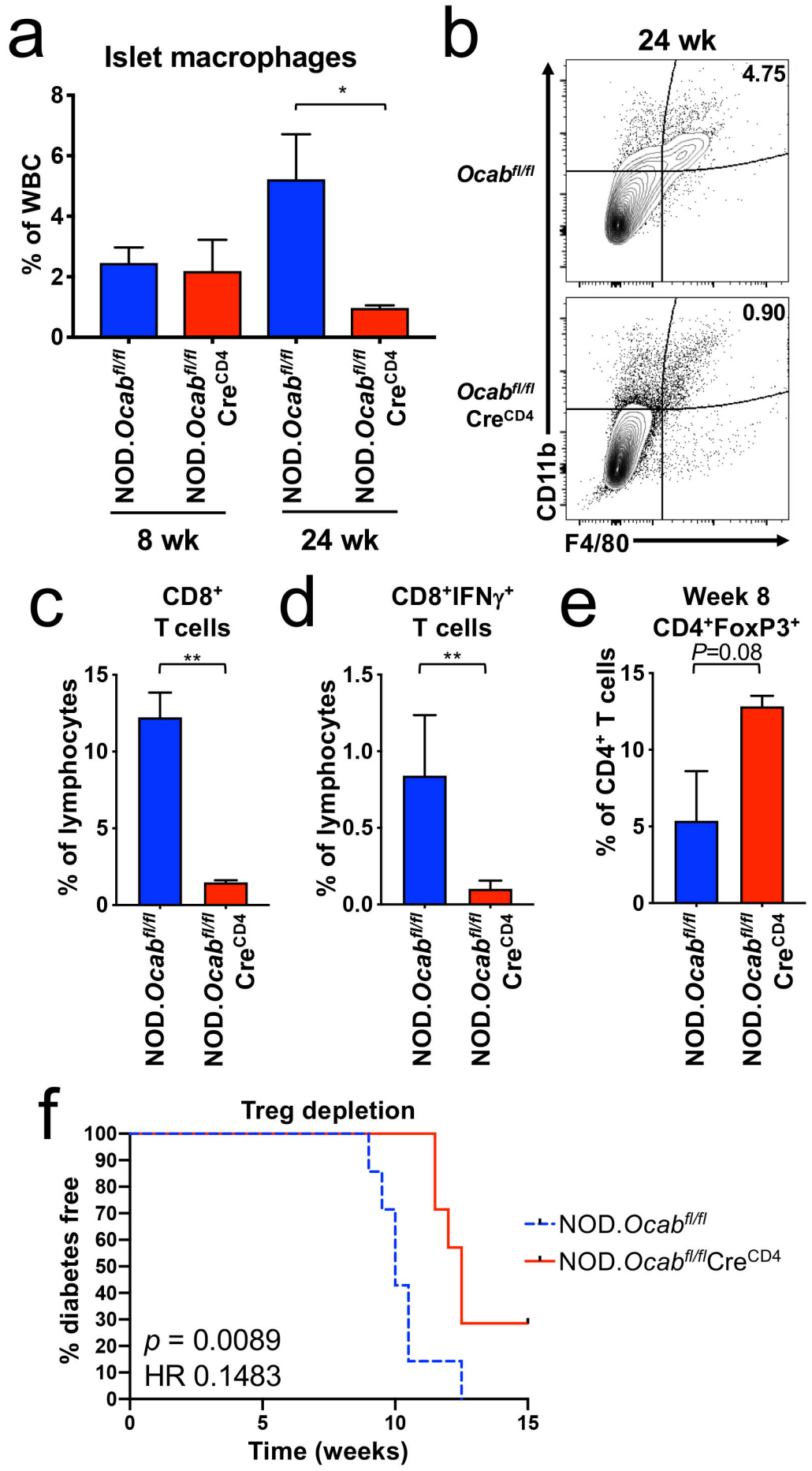

Kim et al. Figure 3

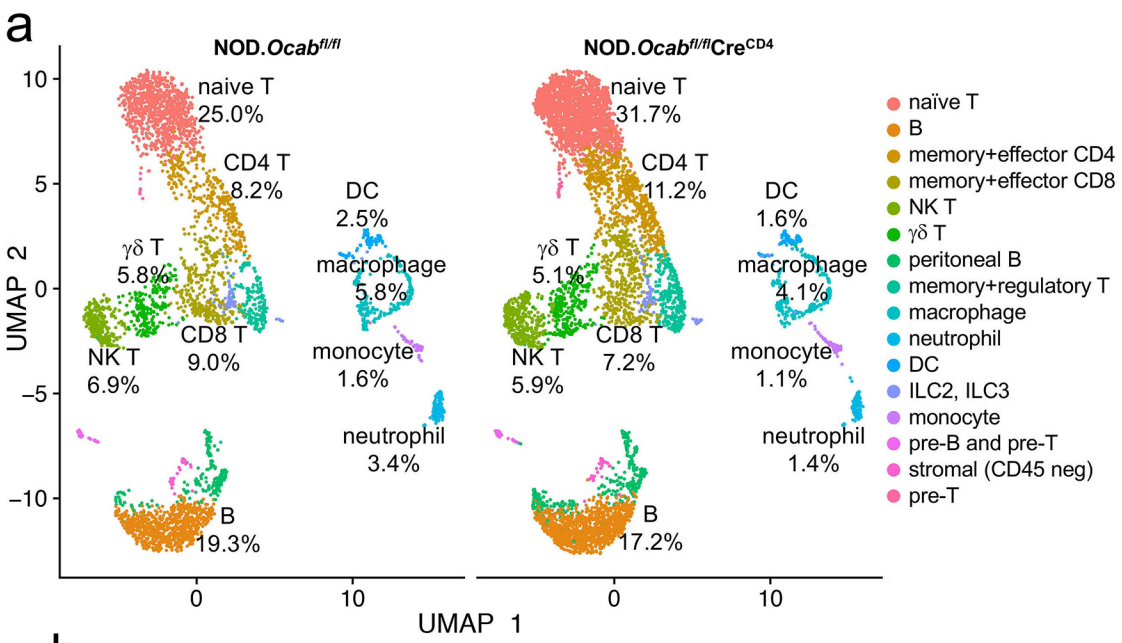

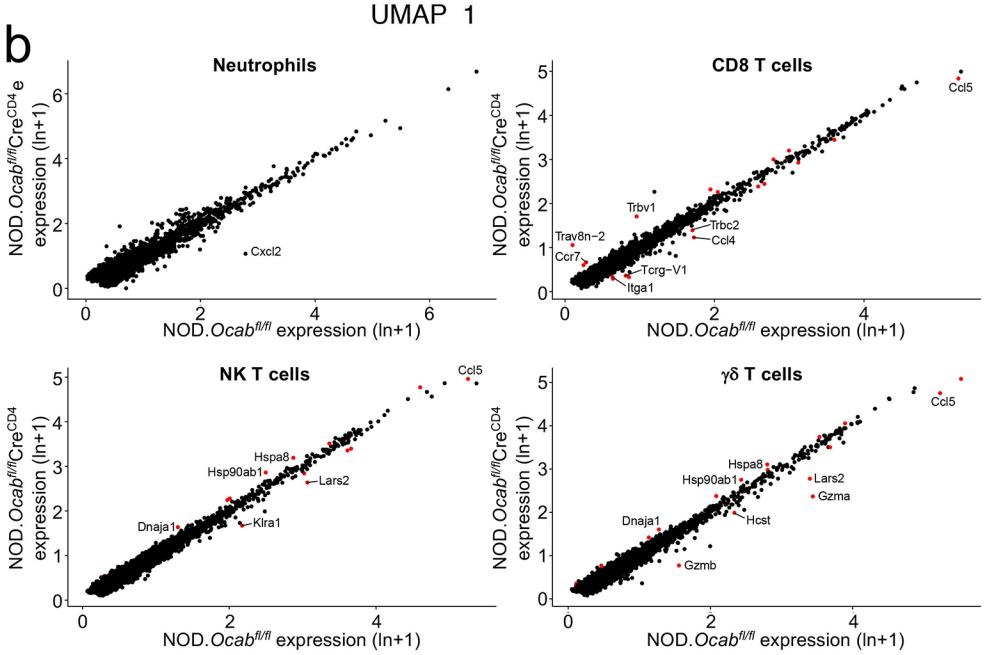

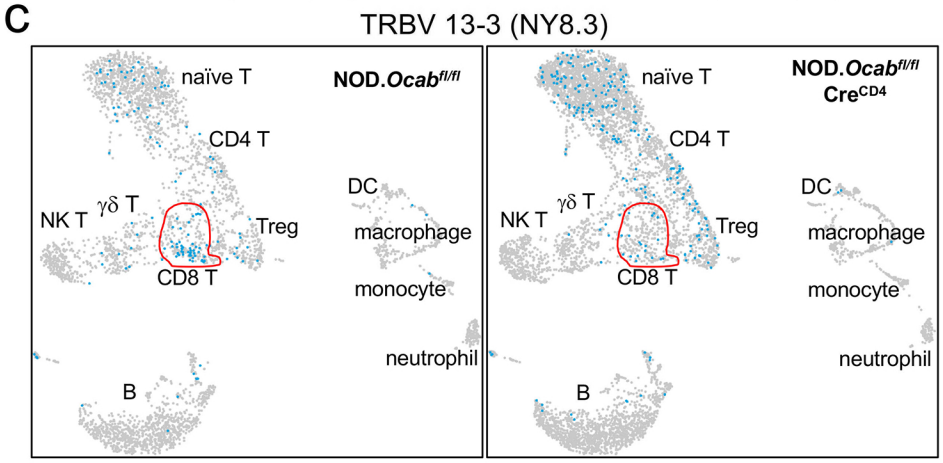

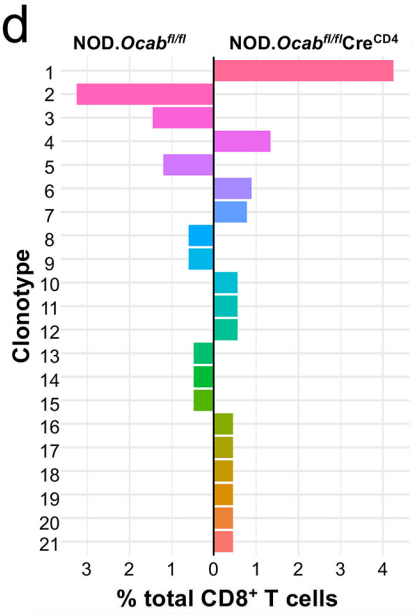

Clonotype	V genes
1	TRAV8N-2;TRBV1;TRBV15
2	TRAV16N;TRBV13-3
3	TRAV9-1;TRBV3
4	TRAV13-1;TRAV16N;TRBV15
5	TRBV13-3

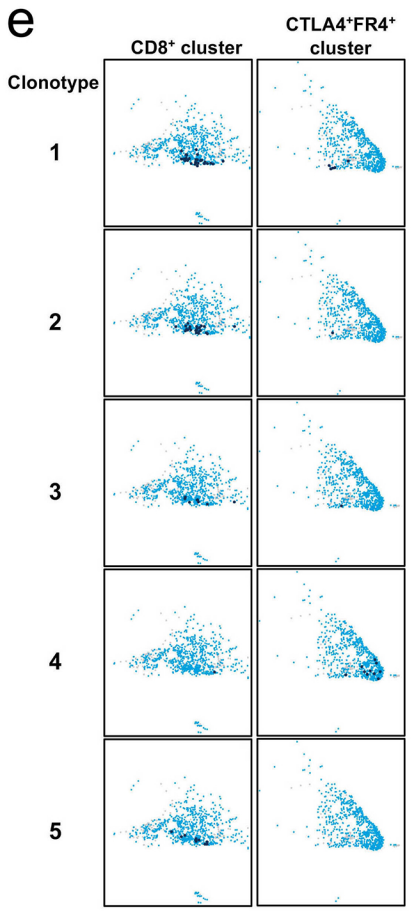

Kim et al. Figure 4

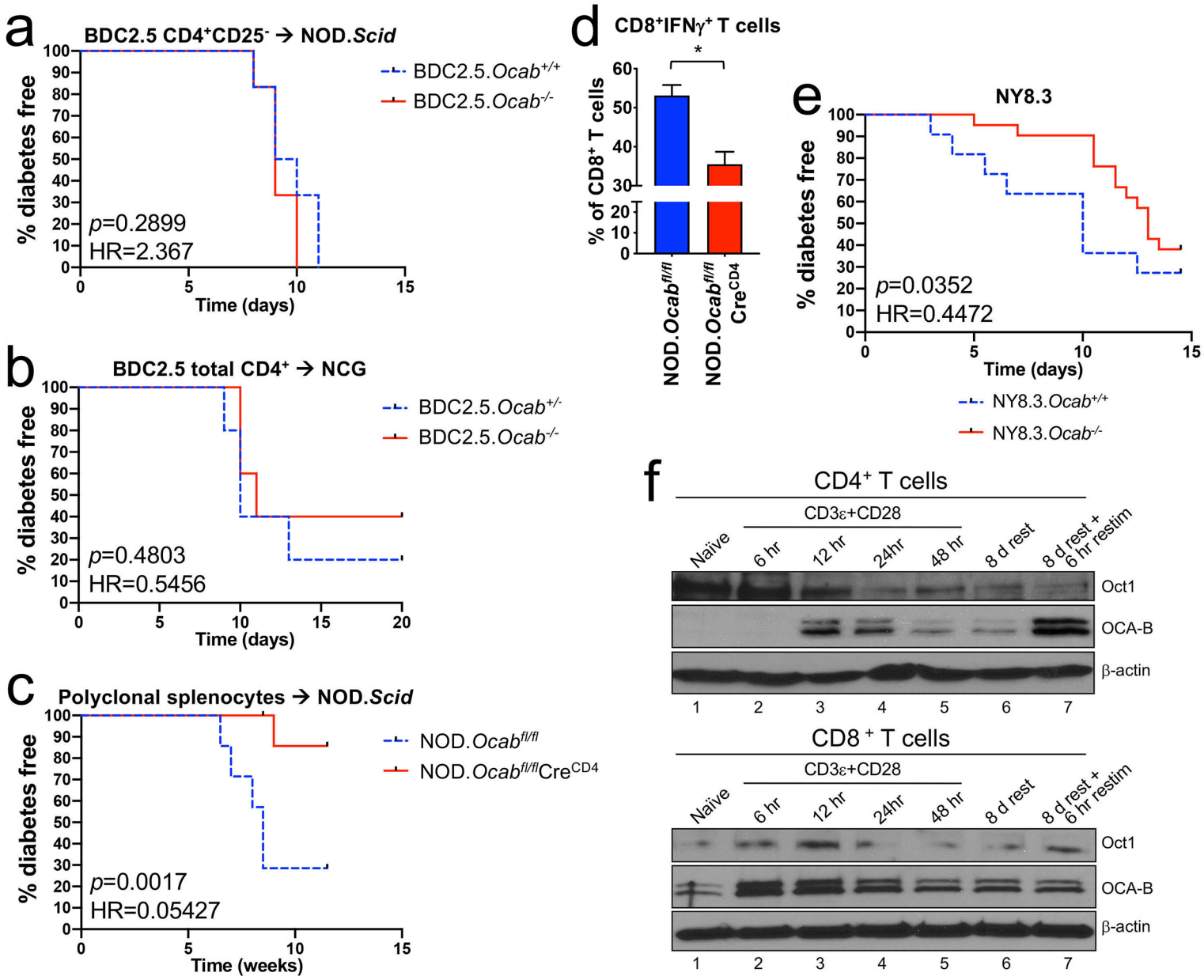

Kim et al. Figure 5

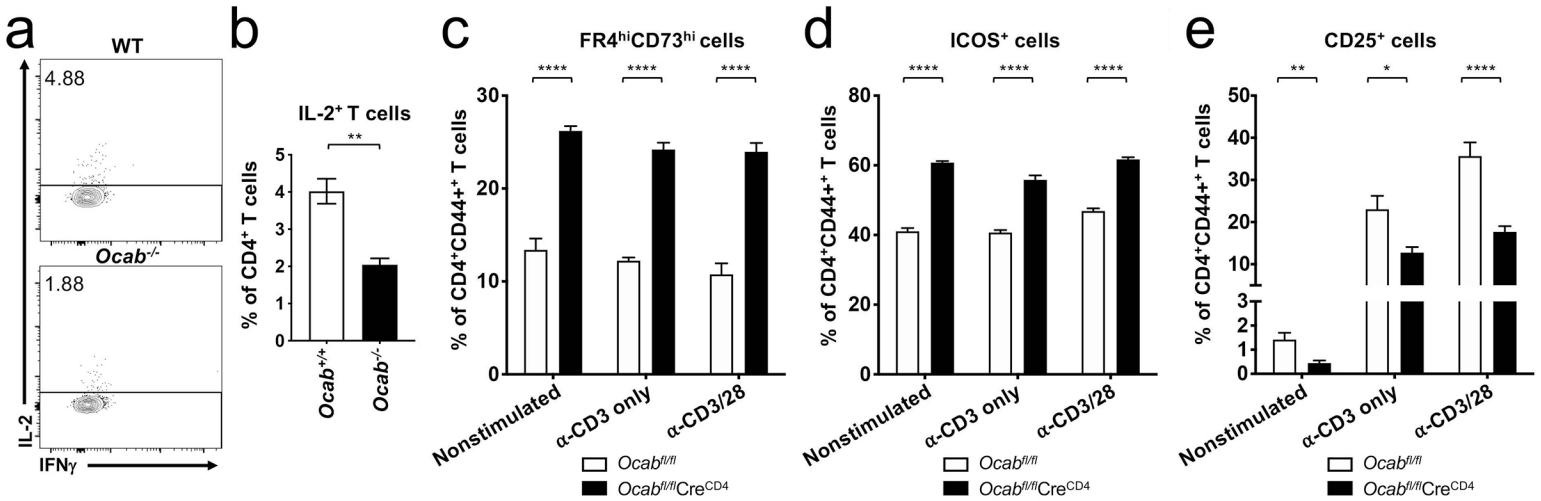

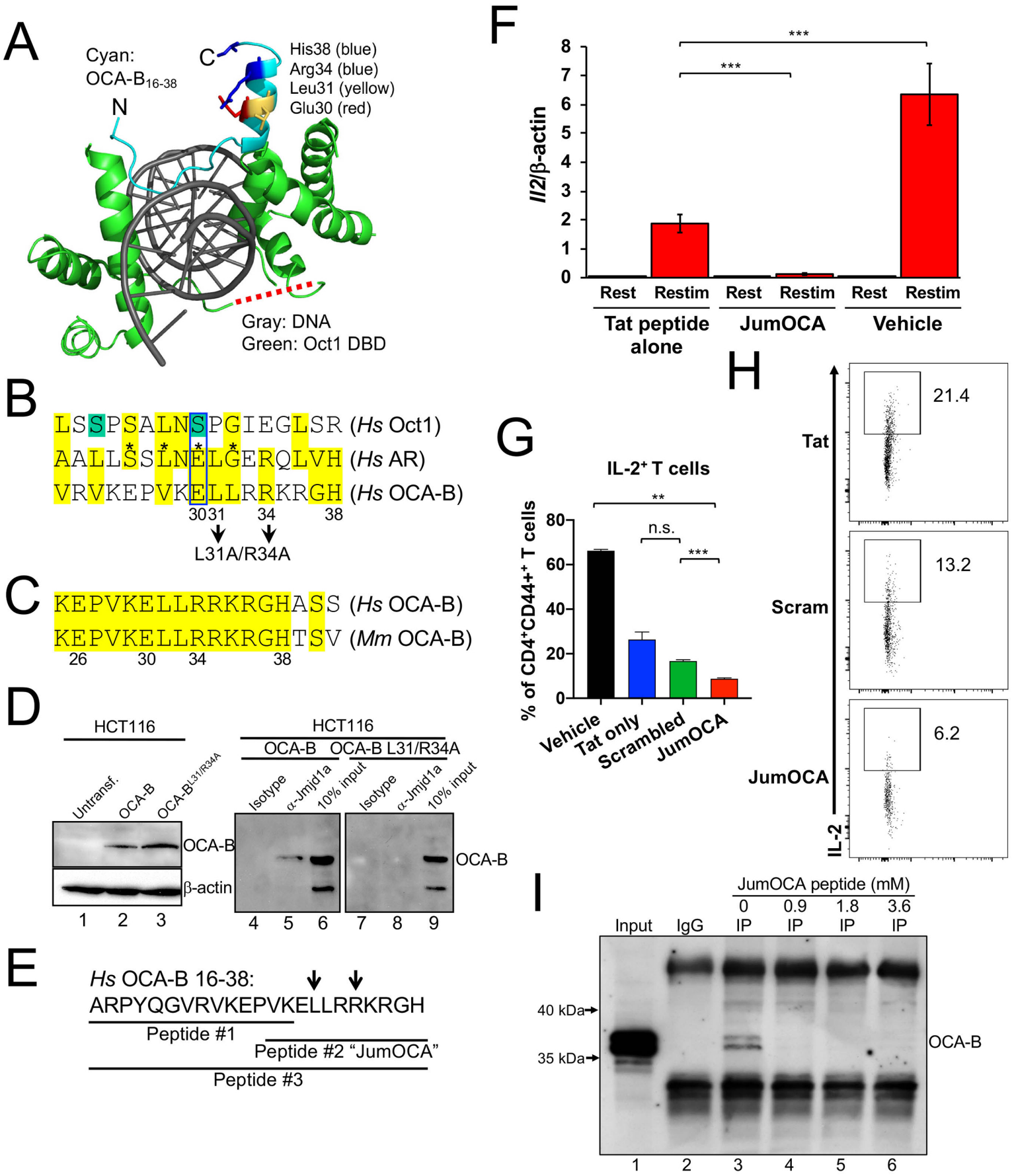
A
Cyan:
OCA-B16-38
C
N
His38 (blue)
Arg34 (blue)
Leu31 (yellow)
Glu30 (red)
Gray: DNA
Green: Oct1 DBD
B
LSSPSALNSPGIEGLSR (Hs Oct1)
AALLSSLNELGERQLVH (Hs AR)
VRVKEPVKELLRRKRGH (Hs OCA-B)
30 31 34 38
L31A/R34A
C
KEPVKELLRRKRGHASS (Hs OCA-B)
KEPVKELLRRKRGHTSV (Mm OCA-B)
26 30 34 38
D
HCT116
Untransf.
OCA-B
OCA-BL31/R34A
OCA-B
β-actin
1 2 3
HCT116
OCA-B
OCA-B L31/R34A
Isotype
α-Jmjd1a
10% input
OCA-B
4 5 6 7 8 9
E
Hs OCA-B 16-38:
ARPYQGVRVKEPVKELLRRKRGH
Peptide #1
Peptide #2 "JumOCA"
Peptide #3
F
Il2/β-actin
Rest
Restim
Tat peptide alone
JumOCA
Vehicle
G
IL-2+ T cells
% of CD4+CD44++ T cells
Vehicle
Tat only
Scrambled
JumOCA
n.s.
H
Tat
Scram
JumOCA
IL-2
21.4
13.2
6.2
I
JumOCA peptide (mM)
0 0.9 1.8 3.6
Input
IgG
IP
40 kDa
35 kDa
OCA-B
1 2 3 4 5 6
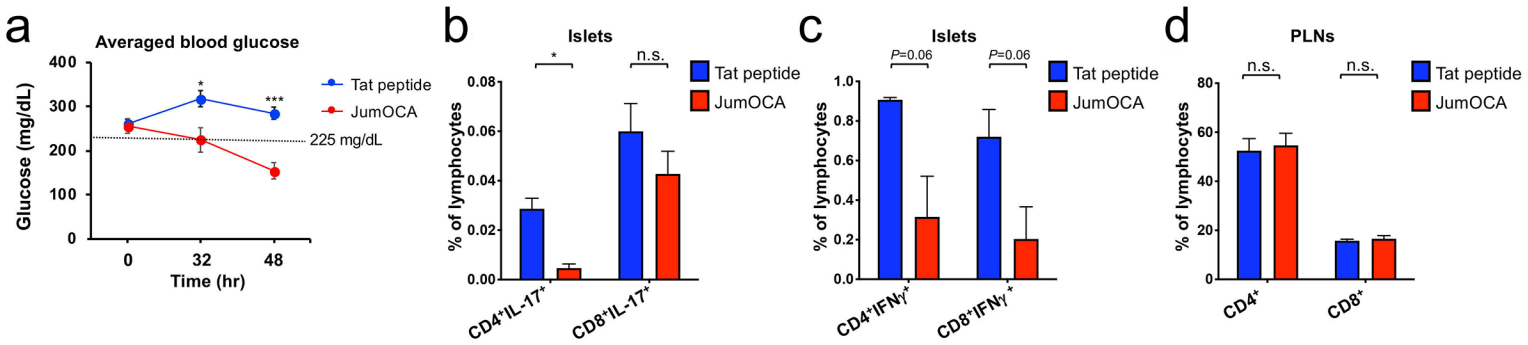
Kim et al. Figure 7